57. Gidekel S, Pizov G, Bergman Y, et al. Oct-3/4 is a dose-dependent oncogenic fate determinant. *Cancer Cell* 2003;4:361–370.
58. Hochedlinger K, Yamada Y, Beard C, et al. Ectopic expression of Oct-4 blocks progenitor-cell differentiation and causes dysplasia in epithelial tissues. *Cell* 2005;121:465–477.
59. Lin CY, Loven J, Rahl PB, et al. Transcriptional amplification in tumor cells with elevated c-Myc. *Cell* 2012;151:56–67.
60. Kim J, Chu J, Shen X, et al. An extended transcriptional network for pluripotency of embryonic stem cells. *Cell* 2008;132:1049–1061.
61. Amit M, Carpenter MK, Inokuma MS, et al. Clonally derived human embryonic stem cell lines maintain pluripotency and proliferative potential for prolonged periods of culture. *Dev Biol* 2000;227:271–278.
62. Thomson JA, Itskovitz-Eldor J, Shapiro SS, et al. Embryonic stem cell lines derived from human blastocysts. *Science* 1998;282:1145–1147.
63. Hiyama E, Hiyama K. Telomere and telomerase in stem cells. *British journal of cancer* 2007;96: 1020–1024.
64. Sperger JM, Chen X, Draper JS, et al. Gene expression patterns in human embryonic stem cells and human pluripotent germ cell tumors. *Proc Natl Acad Sci USA* 2003;100:13350–13355.
65. Ben-Porath I, Thomson MW, Carey VJ, et al. An embryonic stem cell-like gene expression signature in poorly differentiated aggressive human tumors. *Nat Genet* 2008;40:499–507.
66. Wong DJ, Liu H, Ridky TW, et al. Module map of stem cell genes guides creation of epithelial cancer stem cells. *Cell Stem Cell* 2008;2:333–344.
67. Calvanese V, Horrillo A, Hmadcha A, et al. Cancer genes hypermethylated in human embryonic stem cells. *PloS One* 2008;3:e3294.
68. Ben-David U, Benvenisty N. The tumorigenicity of human embryonic and induced pluripotent stem cells. *Nat Rev Cancer* 2011;11:268–277.
69. Ushijima T. Epigenetic field for cancerization. *J Biochem Mol Biol* 2007;40:142–150.
70. Hussein SM, Batada NN, Vuoristo S, et al. Copy number variation and selection during reprogramming to pluripotency. *Nature* 2011; 471:58–62.
71. Gore A, Li Z, Fung HL, et al. Somatic coding mutations in human induced pluripotent stem cells. *Nature* 2011;471:63–67.
72. Lister R, Pelizzola M, Kida YS, et al. Hotspots of aberrant epigenomic reprogramming in human induced pluripotent stem cells. *Nature* 2011;471: 68–73.
73. Pera MF. Stem cells: The dark side of induced pluripotency. *Nature* 2011;471:46–47.
74. Laurent LC, Ulitsky I, Slavin I, et al. Dynamic changes in the copy number of pluripotency and cell proliferation genes in human ESCs and iPSCs during reprogramming and time in culture. *Cell Stem Cell* 2011;8:106–118.
75. Pick M, Stelzer Y, Bar-Nur O, et al. Clone- and gene-specific aberrations of parental imprinting in human induced pluripotent stem cells. *Stem Cells* 2009;27:2686–2690.
76. Stadtfeld M, Apostolou E, Akutsu H, et al. Aberrant silencing of imprinted genes on chromosome 12qF1 in mouse induced pluripotent stem cells. *Nature* 2010;465:175–181.
77. Jirtle RL. Genomic imprinting and cancer. *Exp Cell Res* 1999;248:18–24.
78. Lim DH, Maher ER. Genomic imprinting syndromes and cancer. *Adv Genet* 2010;70: 145–175.
79. Nakagawa M, Takizawa N, Narita M, et al. Promotion of direct reprogramming by transformation-deficient Myc. *Proc Natl Acad Sci USA* 2010;107:14152–14157.
80. Maekawa M, Yamaguchi K, Nakamura T, et al. Direct reprogramming of somatic cells is promoted by maternal transcription factor Glis1. *Nature* 2011;474:225–229.
81. Ramos-Mejia V, Munoz-Lopez M, Garcia-Perez JL, et al. iPSC lines that do not silence the expression of the ectopic reprogramming factors may display enhanced propensity to genomic instability. *Cell Res* 2010;20:1092–1095.
82. Foster KW, Liu Z, Nail CD, et al. Induction of KLF4 in basal keratinocytes blocks the proliferation-differentiation switch and initiates squamous epithelial dysplasia. *Oncogene* 2005; 24:1491–1500.
83. Zhou H, Wu S, Joo JY, et al. Generation of induced pluripotent stem cells using recombinant proteins. *Cell Stem Cell* 2009;4: 381–384.
84. Kim D, Kim CH, Moon JI, et al. Generation of human induced pluripotent stem cells by direct delivery of reprogramming proteins. *Cell Stem Cell* 2009;4:472–476.
85. Warren L, Manos PD, Ahfeldt T, et al. Highly efficient reprogramming to pluripotency and directed differentiation of human cells with synthetic modified mRNA. *Cell Stem Cell* 2010; 7:618–630.
86. Fusaki N, Ban H, Nishiyama A, et al, Hasegawa M. Efficient induction of transgene-free human pluripotent stem cells using a vector based on Sendai virus, an RNA virus that does not integrate into the host genome. *Proc Jpn Acad Ser B Phys Biol Sci* 2009;85: 348–362.
87. Woltjen K, Hamalainen R, Kibschull M, et al. Transgene-free production of pluripotent stem cells using piggyBac transposons. *Methods Mol Biol* 2011;767:87–103.
88. Kaji K, Norrby K, Paca A, et al. Virus-free induction of pluripotency and subsequent excision of reprogramming factors. *Nature* 2009; 458:771–775.
89. Okita K, Nakagawa M, Hyenjong H, et al. Generation of mouse induced pluripotent stem cells without viral vectors. *Science* 2008;322: 949–953.
90. McKinnell RG, Deggins BA, Labat DD. Transplantation of pluripotential nuclei from triploid frog tumors. *Science* 1969;165: 394–396.
91. Hochedlinger K, Blelloch R, Brennan C, et al. Reprogramming of a melanoma genome by nuclear transplantation. *Genes Dev* 2004;18: 1875–1885.
92. Carette JE, Pruszak J, Varadarajan M, et al. Generation of iPSCs from cultured human malignant cells. *Blood* 2010;115: 4039–4042.
93. Kumano K, Arai S, Hosoi M, et al. Generation of induced pluripotent stem cells from primary chronic myelogenous leukemia patient samples. *Blood* 2012;119:6234–6242.
94. Utikal J, Maherali N, Kulalert W, et al. Sox2 is dispensable for the reprogramming of melanocytes and melanoma cells into induced pluripotent stem cells. *J Cell Sci* 2009;122: 3502–3510.
95. Miyoshi N, Ishii H, Nagai K, et al. Defined factors induce reprogramming of gastrointestinal cancer cells. *Proc Natil Acad Sci USA* 2010;107: 40–45.
96. Sieber OM, Tomlinson SR, Tomlinson IP. Tissue, cell and stage specificity of (epi)mutations in cancers. *Nat Rev Cancer* 2005; 5:649–655.
97. Luo J, Solimini NL, Elledge SJ. Principles of cancer therapy: oncogene and non-oncogene addiction. *Cell* 2009;136:823–837.
98. Krivtsov AV, Twomey D, Feng Z, et al. Transformation from committed progenitor to leukaemia stem cell initiated by MLL-AF9. *Nature* 2006;442:818–822.
99. Boyer LA, Lee TI, Cole MF, et al. Core transcriptional regulatory circuitry in human embryonic stem cells. *Cell* 2005;122:947–956.
100. Boyer LA, Plath K, Zeitlinger J, et al. Polycomb complexes repress developmental regulators in murine embryonic stem cells. *Nature* 2006;441: 349–353.
101. Hochedlinger K, Jaenisch R. Monoclonal mice generated by nuclear transfer from mature B and T donor cells. *Nature* 2002;415: 1035–1038.
102. Barker N, Ridgway RA, van Es JH, et al. Crypt stem cells as the cells-of-origin of intestinal cancer. *Nature* 2009;457:608–611.

Development 140, 66-75 (2013) doi:10.1242/dev.084103

Dose-dependent roles for canonical Wnt signalling in *de novo* crypt formation and cell cycle properties of the colonic epithelium

Akihiro Hirata[1,*], Jochen Utikal[2,3,*], Satoshi Yamashita[4], Hitomi Aoki[5], Akira Watanabe[6], Takuya Yamamoto[6], Hideyuki Okano[7], Nabeel Bardeesy[2], Takahiro Kunisada[5], Toshikazu Ushijima[4], Akira Hara[8], Rudolf Jaenisch[9], Konrad Hochedlinger[2,‡] and Yasuhiro Yamada[6,10,‡]

SUMMARY

There is a gradient of β-catenin expression along the colonic crypt axis with the highest levels at the crypt bottom. In addition, colorectal cancers show a heterogeneous subcellular pattern of β-catenin accumulation. However, it remains unclear whether different levels of Wnt signalling exert distinct roles in the colonic epithelium. Here, we investigated the dose-dependent effect of canonical Wnt activation on colonic epithelial differentiation by controlling the expression levels of stabilised β-catenin using a doxycycline-inducible transgenic system in mice. We show that elevated levels of Wnt signalling induce the amplification of Lgr5+ cells, which is accompanied by crypt fission and a reduction in cell proliferation among progenitor cells. By contrast, lower levels of β-catenin induction enhance cell proliferation rates of epithelial progenitors without affecting crypt fission rates. Notably, slow-cycling cells produced by β-catenin activation exhibit activation of Notch signalling. Consistent with the interpretation that the combination of Notch and Wnt signalling maintains crypt cells in a low proliferative state, the treatment of β-catenin-expressing mice with a Notch inhibitor turned such slow-cycling cells into actively proliferating cells. Our results indicate that the activation of the canonical Wnt signalling pathway is sufficient for *de novo* crypt formation, and suggest that different levels of canonical Wnt activations, in cooperation with Notch signalling, establish a hierarchy of slower-cycling stem cells and faster-cycling progenitor cells characteristic for the colonic epithelium.

KEY WORDS: Wnt signalling, Notch signalling, Intestinal stem cell, Mouse

INTRODUCTION

The intestinal epithelium is characterised by rapid and continuous renewal throughout life. One of the major players involved in the renewal of the intestinal epithelium is the canonical Wnt signalling pathway. Experimental manipulation of Wnt signalling has been shown to influence epithelial proliferation in the intestines (Korinek et al., 1998; Pinto et al., 2003; Kuhnert et al., 2004; Sansom et al., 2004; Andreu et al., 2005; Fevr et al., 2007). For example, inactivation of Wnt signalling by transgenic or adenoviral expression of *Dickkopf1* (*Dkk1*), a secreted Wnt inhibitor, leads to marked inhibition of epithelial proliferation in the intestines (Pinto et al., 2003; Kuhnert et al., 2004). By contrast, two independent groups have demonstrated that loss of *Apc* results in a rapid and dramatic enlargement of the crypt compartment associated with abnormal cell proliferation in the small intestine (Sansom et al., 2004; Andreu et al., 2005). Together, these experiments provide definitive evidence for the importance of Wnt signalling in controlling intestinal epithelial proliferation.

In addition to controlling cell proliferation, a role for Wnt/β-catenin signalling in stem cell maintenance in the intestine has been suggested. Inactivation of Wnt signalling by either overexpression of *Dkk1* or conditional deletion of *Ctnnb1* (the gene encoding β-catenin) results in the loss of intestinal crypts, indicating that Wnt signalling is indispensable for stem cell maintenance (Pinto et al., 2003; Kuhnert et al., 2004; Fevr et al., 2007). In fact, the intestinal stem cell (ISC) marker *Lgr5* has initially been identified as a target of β-catenin/Tcf transcription (Barker et al., 2007), which is in accordance with the view that ISCs harbour a higher activity of canonical Wnt signals. In further support of this notion, nuclear accumulation of β-catenin has been observed at the crypt bottom in cells that potentially include ISCs (van de Wetering et al., 2002).

The number of ISCs has to be tightly regulated in the intestinal crypts in order to facilitate tissue turnover but prevent abnormal growth. ISCs are usually involved in a process of homeostatic self-renewal in the adult intestine but can also be rapidly recruited to repair tissues after injury. Indirect evidence for an involvement of Wnt signalling in stem cell amplification derives from a study showing that PTEN deficiency increases the frequency of crypt fission/budding and the number of cells expressing *Musashi1*, a putative ISC marker, through activated Wnt signalling (He et al., 2007). However, the underlying mechanism by which activated Wnt signalling may expand ISCs remains elusive, and direct evidence

[1]Division of Animal Experiment, Life Science Research Center, Gifu University, 1-1 Yanagido, Gifu, 501-1194, Japan. [2]Massachusetts General Hospital Cancer Center and Center for Regenerative Medicine, Harvard Stem Cell Institute, 185 Cambridge Street, Boston, MA 02114, USA. [3]Skin Cancer Unit, German Cancer Research Center, Heidelberg, Germany and Department of Dermatology, Venereology and Allergology, University Medical Center Mannheim, Ruprecht-Karl University of Heidelberg, Mannheim, Germany. [4]Division of Epigenomics, National Cancer Center Research Institute, 5-1-1 Tsukiji, Chuo-ku, Tokyo, Japan. [5]Department of Tissue and Organ Development and [8] Department of Tumor Pathology, Gifu University Graduate School of Medicine, 1-1 Yanagido, Gifu, 501-1194, Japan. [6]Center for iPS Cell Research and Application (CiRA), Institute for Integrated Cell-Material Sciences (WPI-iCeMS), Kyoto University, 53 Kawahara-cho, Shogoin, Sakyo-ku, Kyoto 606-8507, Japan. [7]Department of Physiology, Keio University School of Medicine, 35 Shinanomach, Shinjuku-ku, Tokyo 160-8582, Japan. [9]Whitehead Institute for Biomedical Research, Massachusetts Institute of Technology, Cambridge, MA 02142, USA. [10]PRESTO, Japan Science and Technology Agency, Saitama, Japan.

*These authors contributed equally to this work
‡Authors for correspondence (khochedlinger@helix.mgh.harvard.edu; y-yamada@cira.kyoto-u.ac.jp)

Accepted 15 October 2012

that elevated Wnt signalling is sufficient for stem cell expansion in the adult intestine is lacking.

Disruption of canonical Wnt signalling is involved in the vast majority of colon cancers. Mutation in *APC* or *CTNNB1* is the initiating event in the transformation of colonic epithelial cells, which lead to the constitutive activation of Wnt signalling. Importantly, despite the presence of the activating mutations for Wnt signalling, colorectal cancers show cellular heterogeneity of β-catenin accumulation within a tumour mass. Immunohistochemical studies have revealed that nuclear β-catenin accumulation, the hallmark of activated Wnt signalling, is observed in a subset of colon tumour cells (Brabletz et al., 2001; Jung et al., 2001; Fodde and Brabletz, 2007). Furthermore, a recent study indicates that colon tumour cells with high Wnt signalling activity show the properties of cancer stem cells (Vermeulen et al., 2010), which emphasises the need for further studies on the dose-dependent effect of Wnt signalling on intestinal epithelial cells.

Although a large body of literature has established that activation of the canonical Wnt signalling is the dominant force in the maintenance of intestinal homeostasis, other signalling cascades, such as the Notch, BMP and PI3 cascades, have also been implicated in the control of epithelial cell proliferation and stem cell turnover (Scoville et al., 2008). However, it remains poorly understood how these other signalling cascades integrate with Wnt signalling in the intestinal epithelium to control stem cell turnover and epithelial regeneration. It is assumed that the various signalling cascades act in a hierarchical manner, and regulate each other. A better understanding of how the coordinated activity of these signalling cascades maintains intestinal homeostasis is crucial for dissecting the mechanisms of ISCs as well as for attempts to utilise stem cells in regenerative medicine and to target them in diseases such as cancer.

Using a novel β-catenin-inducible mouse model, we show here that elevated levels of activated β-catenin induces *de novo* crypt formation but reduces epithelial cell proliferation among progenitors. However, combined β-catenin overexpression and Notch inhibition turns these slow-cycling cells into proliferating cells. These results imply that β-catenin signalling fulfils dual roles in the control of intestinal epithelial regeneration by (1) promoting crypt formation and (2) activating cell proliferation in cooperation with Notch signalling.

MATERIALS AND METHODS

Mice

Transgenic mice expressing histone H2B-green fluorescent protein (H2B-GFP) fusion protein under the control of a TRE were obtained from Jackson Laboratories [Bar Harbor, ME, USA; strain name: Tg(tetO-HIST1H2BJ/GFP)47Efu] and crossed with mice harbouring a ROSA26 promoter-driven M2rtTA allele (Beard et al., 2006). β-Catenin embryonic stem (ES) cell line was generated with stabilised β-catenin (S33 mutation) cDNA (Morin et al., 1977; van Noort et al., 2002) with use of KH2 ES cell line and injected into blastocysts to produce transgenic mice. Mice of 4 to 8 weeks of age were fed 0.1 or 2.0 mg/ml doxycycline in the drinking water supplemented with 10 mg/ml sucrose. *Lgr5-GFP* knock-in mouse were obtained from Jackson Laboratories (strain name: B6.129P2-*Lgr5*$^{tm1(cre/ESR1)Cle}$/J).

Crypt isolation

Crypts were isolated form the whole colon and caecum by incubation in Hanks' balanced salt solution containing 30 mM EDTA as described previously (Tsukamoto et al., 2001).

Flow cytometry

Isolated crypts were incubated in 1% collagenase type 1 for 15 minutes at 37°C and then 0.25% trypsin/1m M EDTA for 5 minutes at 37°C. Single-cell suspensions were obtained by transfer through nylon mesh to remove large clumps, washing, and resuspension in staining medium containing 0.5 μl/ml propidium iodide (Calbiochem-Novabiochem Corp., San Diego, CA, USA) to eliminate dead cells. The cells were sorted by fluorescence-activated cell sorting (FACS) using a Vantage SE flow cytometer (Becton Dickinson, San Jose, CA, USA).

Microarray analysis

Total RNA was extracted from isolated crypts or FACS-sorted cells as previously reported (Yamashita et al., 2003). Oligonucleotide microarray hybridisation and scanning using GeneChip Mouse Genome 430 2.0 Array (Affimetrix) were performed as previously reported (Yamashita et al., 2003). For the pathway analysis, 907 probe sets, which are specifically upregulated in β-catenin induced cells, but not in H2B-low fast-cycling cells, were selected. The gene enrichment analysis was performed with DAVID PANTHER annotation tool. Microarray data have been deposited in Gene Expression Omnibus database under accession number GSE41688.

Quantitative real-time RT-PCR

qRT-PCR was performed as described previously (Oyama et al., 2008). The expression level of each gene was normalised to the β-actin expression level using the standard curve method. Each experiment was done in either duplicate or triplicate, and then, the average was calculated. Primer sequences for qPCR were taken from PrimerBank. The primer sequences are listed in supplementary material Table S2.

Histological and immunohistochemical analysis

Normal and tumour tissue samples were fixed in 10% buffered formalin, proceeded by standard method and embedded in paraffin. Sections were stained with Haematoxylin and Eosin (H&E), and serial sections were used for immunohistochemical analysis. Immunostaining was performed as described previously (Oyama et al., 2008) using the following antibodies: anti-β-catenin (1:1000 dilution; BD Transduction Laboratories, San Diego, CA, USA), anti-Musashi-1 [1:500 dilution (Kaneko et al., 2000)], anti-BrdU (1:250 dilution; Abcam, Cambridge, UK), anti-Hes1 [1:100 dilution; a gift from Dr Sudo (Ito et al., 2000)], anti-GFP (1:1500 dilution; Invitrogen, Carlsbad, CA, USA), anti-Ki67 (1:250 dilution; Dako Corp., Carpinteria, CA, USA) and anti-chromogranin A (1:1500 dilution; Abcam). Photomicrographs show the distal part of the colon or caecum in the figures.

Bromodeoxyuridine (BrdU) assay

Mice were injected with BrdU intraperitoneally (i.p.) at a dose of 100 mg/kg body weight. Mice were sacrificed 2 or 48 hours after injection, and incorporated BrdU was detected by immunostaining with anti-BrdU antibody as described above.

Notch inhibitor

γ-Secretase inhibitor (MRK003-ONC) was kindly provided by Merck and administrated orally at 100 mg/kg 2 days before sacrifice.

RESULTS

Canonical Wnt signalling is physiologically active in proliferative compartment of colonic crypts

Previous studies have shown by experimental manipulation of the Wnt signalling cascade that canonical Wnt signalling regulates intestinal epithelial proliferation (Korinek et al., 1998; Pinto et al., 2003; Kuhnert et al., 2004; Sansom et al., 2004; Andreu et al., 2005; Fevr et al., 2007). However, whether canonical Wnt signalling is active in the proliferative compartment of normal colonic crypts remains unclear. To address this question, we separated actively proliferating progenitor cells (transit-amplifying cells) from non-proliferating cells in the colon by using transgenic mice that express a histone H2B-GFP fusion protein under the control of a tetracycline-responsive regulatory element (TRE) (Tumbar et al., 2004). H2B-GFP becomes incorporated or diluted in a cell cycle-dependent manner and thus facilitates the separation of frequently dividing cells from infrequently dividing cells in any given tissue,

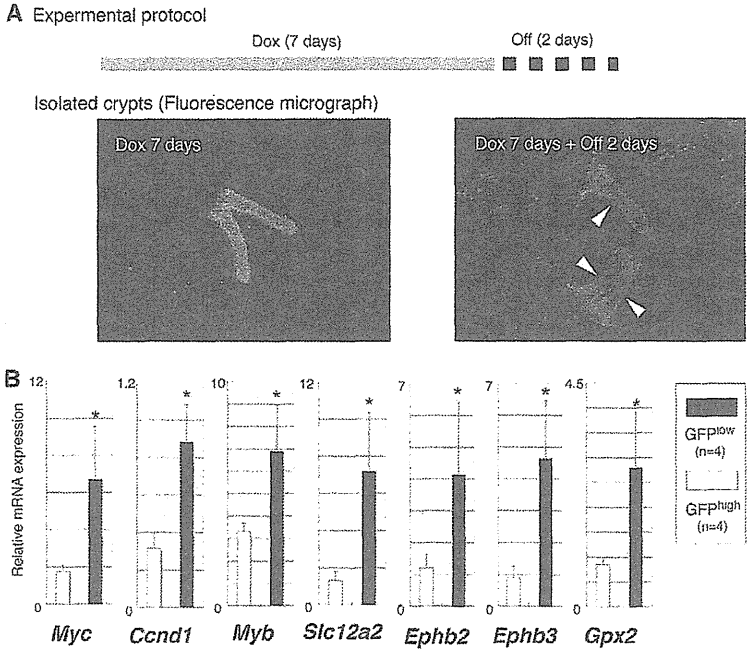

Fig. 1. Upregulation of canonical Wnt target genes in the proliferative compartments of colonic crypts. (**A**) Separation of proliferating cells from non-proliferative cells in the colon of histone H2B-GFP inducible mice. All crypt cells were labelled with nuclear GFP after Histone-GFP induction for 7 days, whereas the subsequent withdrawal of the induction resulted in dilution of the nuclear GFP signals in proliferating progenitor cells according to the cell divisions. Arrowheads indicate the decreased signal of the nuclear GFP at the proliferating compartments. (**B**) qRT-PCR for canonical Wnt target genes in GFP^{low} and GFP^{high} cells. After FACS sorting, the expression of canonical Wnt target genes was analysed by qRT-PCR. Expressions of *Myc*, *Ccnd1*, *Myb*, *Slc12a2*, *Ephb2*, *Ephb3* and *Gpx2* are significantly higher in GFP^{low} cells than in GFP^{high} cells. Data are mean ± s.d.; $^*P<0.05$, by Mann–Whitney *U*-test.

as has been successfully shown for the skin and haematopoietic system (Tumbar et al., 2004; Foudi et al., 2009). Specifically, H2B-GFP mice were crossed with mice harbouring a *Rosa26* promoter-driven M2 reverse tetracycline transactivator (M2rtTA) allele (Beard et al., 2006) to enable H2B expression in essentially all tissues. In the absence of doxycycline treatment, colonic epithelial cells exhibited no detectable GFP signals, thus excluding leaky expression of the transgene. By contrast, 7 days after doxycycline administration, all crypt cells exhibited a strong nuclear GFP signal (Fig. 1A). When doxycycline was withdrawn for 2 days after the initial labelling period, nuclear GFP signal was diluted in proliferating cells, consistent with rapid cell divisions of progenitor cells, whereas non-proliferating cells retained GFP (Fig. 1A). GFP^{high} non-proliferating and GFP^{low} proliferating epithelial cells were then sorted from the isolated crypts by FACS for subsequent molecular analyses (supplementary material Fig. S1A). To validate our approach to separate proliferating cells from non-proliferating cells using H2B-GFP dilution, we examined the expression levels of cell proliferation-related genes by microarray analysis. As expected, the expression of cyclins and Cdks, including *Ccna2*, *Ccnb1*, *Ccnd1*, *Ccnd2*, *Cdk2*, *Cdk4* and *Cdk6*, was higher in GFP^{low} cells than in GFP^{high} cells, whereas Cdk inhibitors, such as *Cdkn1a* and *Cdkn2b*, were found to be downregulated in GFP^{low} cells compared with GFP^{high} cells. Gene expression of candidates was validated by quantitative RT-PCR (supplementary material Fig. S1B). We also confirmed that GFP^{low} cells contained a higher number of Ki-67 (Mki67 – Mouse Genome Informatics)-positive cells than GFP^{high} cells by immunostaining colon sections of H2B-GFP mouse (supplementary material Fig. S1C). Importantly, we found that a number of canonical Wnt signalling target genes were upregulated in GFP^{low} proliferating cells compared with GFP^{high} non-proliferating cells using microarray analysis. qRT-PCR confirmed a significant upregulation of Wnt target genes (van de Wetering et al., 2002) (Fig. 1B), implying that canonical Wnt signalling is associated with active proliferation of progenitor cells in normal colonic crypts.

Forced induction of β-catenin leads to rapid *de novo* crypt formation in the colon

To investigate the effects of acute Wnt activation on adult intestinal homeostasis, we generated doxycycline-inducible β-catenin mice. This was achieved by targeting a constitutive active version of β-catenin (S33 mutation) under the control of a tetOP minimal promoter into the *Col1a1* locus in ES cells, which were subsequently injected into blastocysts to produce transgenic mice. Unless noted, homozygous transgenic mice were used in the experiment. When we fed adult mice doxycycline in the drinking water (2.0 mg/ml), β-catenin-induced animals became morbid after only 6-8 days. In the colon, 5 days of doxycycline treatment led to nuclear accumulation of β-catenin in the epithelium (Fig. 2A) and strong upregulation of canonical Wnt target genes such as *Myc* and *Ccnd1* (Fig. 2B). Notably, we frequently observed crypt fission and/or branching in β-catenin-induced colon sections, suggesting that the *de novo* crypt formation was induced by β-catenin induction (Fig. 2A). Immunohistological analyses of colon sections from doxycycline-induced chimeric mice demonstrated that the crypt fission/branching phenotype was only seen in β-catenin-induced crypts but not in host embryo-derived crypts, documenting a cell-autonomous effect of β-catenin induction (supplementary material Fig. S2A). We also observed an increase in crypt fission/branching in the crypts of the small intestine (supplementary material Fig. S2B). Analysis of isolated crypts confirmed that the fission and budding of crypts occurred at a significantly higher rate in β-catenin-induced colon than in non-induced colon (Fig. 2C,D). In addition, staining of sections for mucin with Alcian Blue-periodic acid-Schiff (AB-PAS) demonstrated a significant suppression of cellular differentiation towards goblet cells following β-catenin activation (supplementary material Fig. S3A). By contrast, chromogranin A-positive cells were found in both β-catenin-induced and non-induced crypts, showing a lesser effect on the enteroendocrine cell differentiation (supplementary material Fig. S3B). The numbers of chromogranin A-positive cells per crypt were 1.36±1.00 and 1.12±1.10 in β-catenin-induced and non-induced

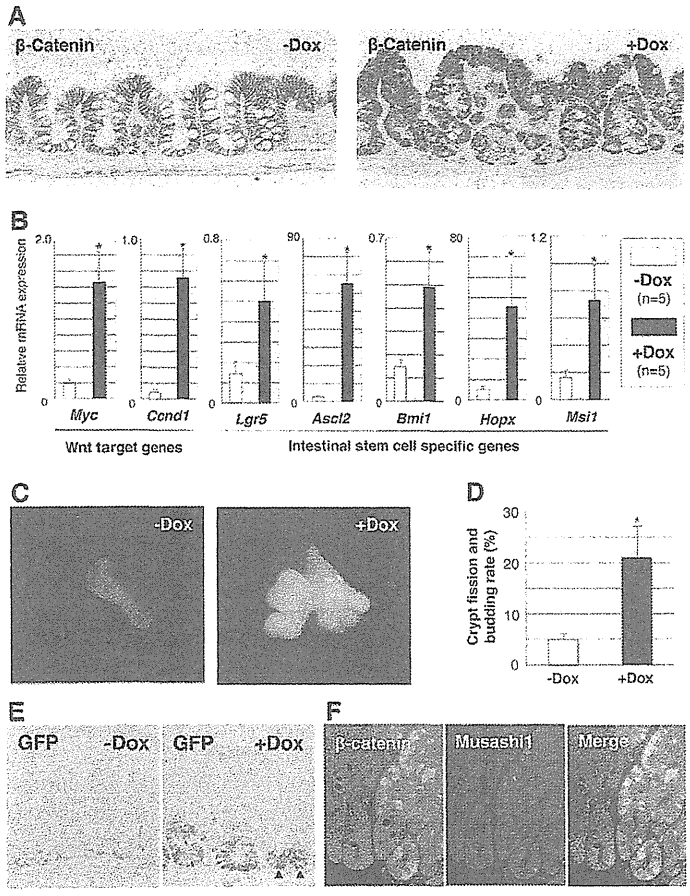

Fig. 2. β-Catenin induction leads to *de novo* crypt formation with increased expression of ISC markers in the colon. (**A**) β-Catenin immunostaining on colonic section of β-catenin-induced mice. Doxycycline treatment results in nuclear accumulation of β-catenin and frequent fission/budding of colonic crypts. (**B**) qRT-PCR for Wnt target genes and ISC-specific genes. The expression of Wnt target genes and ISC-specific genes are significantly upregulated by β-catenin induction. Data are mean ± s.d.; *P<0.05, by Mann–Whitney U-test. (**C**) Isolated colonic crypts from a doxycycline-treated mouse. A drastic crypt budding is observed in the crypt with β-catenin induction. (**D**) Fission/budding rate in isolated crypts from doxycycline-treated mice. Crypt fission/budding occurs at a significantly higher rate in doxycycline-treated mice than in non-treated mice. Data are mean ± s.d.; *P<0.05, by Mann–Whitney U-test. (**E**) Immunostaining for GFP on colonic sections of β-catenin-induced mice with *Lgr5-GFP* knock-in allele. GFP expression reveals an increased number of *Lgr5*-expressing cells at the lower part of colonic crypts in doxycycline-treated mice. Note that GFP-expressing cells are observed at the bottom of a bifurcating crypt (arrowheads). (**F**) Double immunostaining for Musashi1 (red) and β-catenin (green) on a colonic section of a doxycycline-treated chimeric mouse. Musashi1 expression is coincident with increased β-catenin expression.

colonic crypts, respectively, and no statistical significance was found between groups.

Barker et al. demonstrated that in the mouse gastrointestinal tract Lgr5 specifically labels active ISCs, which are located at the crypt base, cycle frequently and replenish the entire epithelium within a week (Barker et al., 2007). Consistent with the fact that *Lgr5* is a target of β-catenin/Tcf transcription (Barker et al., 2007), qRT-PCR demonstrated that β-catenin activation caused a significant increase in *Lgr5* expression (Fig. 2B). To determine whether the number of *Lgr5*-expressing cells has also increased in these mice, we crossed β-catenin-inducible mice with *Lgr5-GFP* knock-in mice, in which the *GFP* gene is regulated by the endogenous *Lgr5* promoter (Barker et al., 2007). Immunohistochemistry for GFP revealed that the number of *Lgr5*-expressing cells had indeed increased by 4.2-fold following β-catenin induction (Fig. 2E; supplementary material Fig. S4). Of note, although nuclear accumulation of β-catenin was observed throughout the crypt epithelium, expanded *Lgr5*-expressing cells were only observed at the lower part of the crypts (Fig. 2E; supplementary material Fig. S4A). This finding suggests that only existing ISCs, and possibly progenitor cells, respond to Wnt activation by producing more *Lgr5*-expressing cells whereas differentiated cells, located at the upper part of the crypts, are unresponsive to forced β-catenin expression. In addition to an increase in *Lgr5* expression, we also observed a strong upregulation of *Ascl2* (Fig. 2B), another active ISC-specific gene (van der Flier et al., 2009). As transgenic expression of *Ascl2* has been recently shown to induce ectopic crypt formation in the intestine (van der Flier et al., 2009), the increased levels of *Ascl2* might explain the observed crypt fission/budding phenotype in β-catenin-induced crypts. In addition to active ISCs, recent reports have indicated that quiescent ISCs are located at position 4 of the small intestine (Li and Clevers, 2010). Interestingly, β-catenin induction increased the expression of markers for the quiescent ISCs as well, including *Bmi1* and *Hopx* (Fig. 2B) (Sangiorgi and Capecchi, 2008; Takeda et al., 2011). Lastly, we examined the expression of Musashi1, a marker for putative stem and early progenitor cells (Potten et al., 2003), and found that β-catenin induction resulted in an upregulation of Musashi1 (Fig. 2B,F) in a cell-autonomous manner (Fig. 2F). Taken together, these data demonstrate that acute activation of β-catenin results in *de novo* crypt formation within a few days in a cell-autonomous fashion, accompanied by the amplification of ISC-like cells.

Colon cells with highest nuclear β-catenin do not actively divide

Previous studies have suggested that the canonical Wnt signalling plays a role in active cell proliferation of the intestine (Sansom et al., 2004; Andreu et al., 2005). In agreement, using the histone H2B-GFP mouse model, we show here that Wnt signalling is active in the proliferating progenitor compartment of normal colonic crypts under physiological conditions (Fig. 1B). To assess directly the effect of Wnt activation on the cell proliferation, we performed double-immunostaining with β-catenin and the proliferation marker Ki-67 on β-catenin-induced colonic sections. Unexpectedly, we found that the majority of cells with nuclear β-catenin failed to stain positively for Ki-67 (Fig. 3A). Instead, Ki-67 staining was

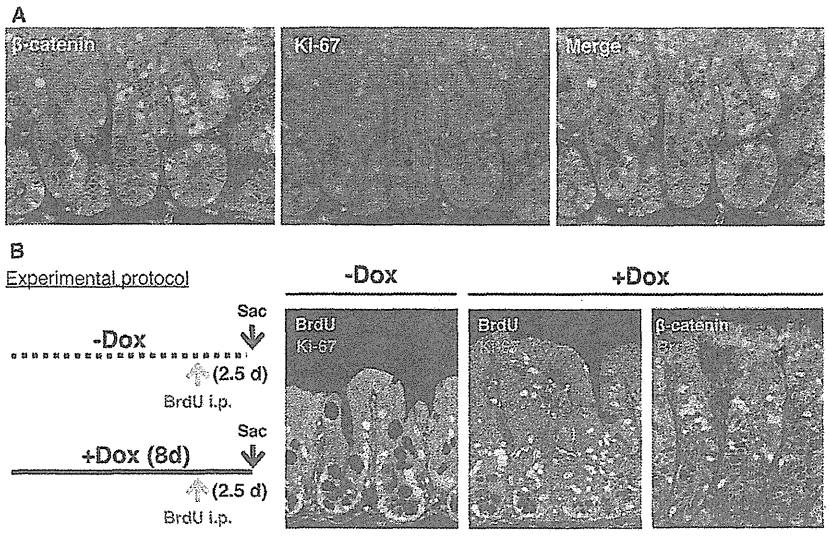

Fig. 3. Slow cycling properties of β-catenin-induced colonic cells. (**A**) Double immunostaining for β-catenin (green) and Ki-67 (red) on a β-catenin-induced colonic section. Majority of colonic cells with strong nuclear β-catenin expression are not coincident with Ki-67. (**B**) A scheme of the BrdU pulse-chase experiment and double immunostaining for Ki-67/BrdU and β-catenin/BrdU. In normal crypts, most proliferating progenitor cells have lost the BrdU retention according to the active cell divisions, and only a small number of cells retain BrdU. By contrast, β-catenin induction leads to an increased number of BrdU-retaining cells. Immunostaining for β-catenin (green) and BrdU (red) shows that BrdU-retaining cells frequently express nuclear β-catenin, indicating that colonic cells with strong nuclear β-catenin divide slowly. Sac, sacrifice.

predominantly observed in cells adjacent to cells with strong nuclear β-catenin signal (Fig. 3A). The majority of Ki-67-positive cells showed cytoplasmic and moderate β-catenin expression (76.7%) on the section, but some Ki-67-positive cells revealed nuclear and strong expression (23.3%). These observations were confirmed by a BrdU incorporation assay. When mice were injected with BrdU (100 mg/kg i.p.) 2 hours before sacrifice, the colonic cells with strong nuclear β-catenin showed less frequent BrdU incorporation (supplementary material Fig. S5A). We infer from this finding that intestinal cells with strong nuclear β-catenin expression did not actively divide. To investigate further the proliferation history of cells after β-catenin induction, we performed a pulse-chase experiment using BrdU (Fig. 3B). Mice were given a single BrdU injection (100 mg/kg i.p.) during the doxycycline treatment and were sacrificed 2 days later (Fig. 3B). β-Catenin induction caused an increased number of BrdU-retaining, i.e. non-dividing, cells near the crypt bottom, whereas non-induced crypts contained a small number of BrdU-retaining cells above the proliferative compartment (Fig. 3B). Furthermore, double-immunostaining for BrdU and β-catenin revealed that BrdU-retaining cells frequently expressed nuclear β-catenin (Fig. 3B). These results imply that, although forced β-catenin activation results in a net increase of cell proliferation in the colon, cells with strong nuclear β-catenin signal divide relatively slowly as measured by Ki-67 proliferation and BrdU label-retention assays. To support these findings, qRT-PCR revealed that the expression of the Cdk inhibitors *Cdkn1a*, *Cdkn1b* and *Cdkn1c* were significantly upregulated in β-catenin-induced colonic crypts (supplementary material Fig. S5B).

β-Catenin overexpression induces activation of Notch

In order to dissect further the molecular mechanisms underlying *de novo* crypt formation upon β-catenin induction, we compared the gene expression profiles of β-catenin-induced and non-induced colon crypts. Briefly, colonic crypts isolated from β-catenin-inducible control mice and from mice fed doxycycline for 5 days were subjected to microarray analysis. Consistent with our finding that β-catenin induction results in *de novo* crypt formation, microarray data confirmed the upregulation of ISC-specific genes, such as *Lgr5*, *Ascl2* and *Hopx*, as well as Wnt target genes in β-catenin-induced colon crypts (supplementary material Table S1).

Next, we wished to elucidate the apparent discrepancy between β-catenin-induced *de novo* crypt formation and the observed slow cycling properties of β-catenin-high cells. To this end, we compared gene expression profiles of β-catenin-induced cells and fast-cycling H2B-GFP low cells. Interestingly, pathway analysis revealed that genes in the Notch signalling pathway are specifically upregulated in β-catenin-induced colonic cells compared with fast-cycling normal crypt cells (Fig. 4A). qRT-PCR confirmed that *Hes1*, a well-established target gene of Notch signalling, is strongly induced by β-catenin activation with significant upregulation of Notch ligands (*Jag1* and *Jag2*) and Notch receptors (*Notch1* and *Notch2*) (Fig. 4B). Furthermore, we found that Notch ligands and Notch receptors were significantly upregulated as early as 12 hours after doxycycline treatment (Fig. 5B; see more details below). Consistent with this observation, immunohistochemical analysis revealed the strong nuclear expression of Hes1 on colonic sections of β-catenin-induced mice. (supplementary material Fig. S6). Our results suggest that β-catenin expression might activate Notch signalling through upregulation of its ligands and receptors.

Notch inhibition induces active cell proliferation in slow-cycling cells and blocks crypt fission and budding by β-catenin induction

In order to determine the relative contribution of activated Notch signalling to *de novo* crypt formation and the slow-cycling properties of colonic cells following β-catenin activation, we treated β-catenin-induced mice with a Notch/γ-secretase inhibitor (Fig. 4C). Surprisingly, treatment with a Notch inhibitor induced active proliferation of β-catenin-expressing, slow-cycling cells. Inhibitor-treated crypts were elongated with increased numbers of Ki-67 positive cells (Fig. 4D,E; supplementary material Fig. S7). Importantly, the simple withdrawal of doxycycline treatment (protocol G4) or the administration of Notch inhibitor alone (protocol G5) did not cause abnormal cell proliferation (Fig. 4E), indicating that constitutive Wnt activation is essential for active cell proliferation. To quantify the effect of Notch inhibition on cell proliferation in the presence of β-catenin activation, we performed a pulse-chase experiment with BrdU. Mice were given a single dose of BrdU (100 mg/kg i.p.) during the doxycycline treatment in the presence or absence of Notch inhibitor, and animals were sacrificed 2 days later. Immunohistochemical analysis showed that, in contrast

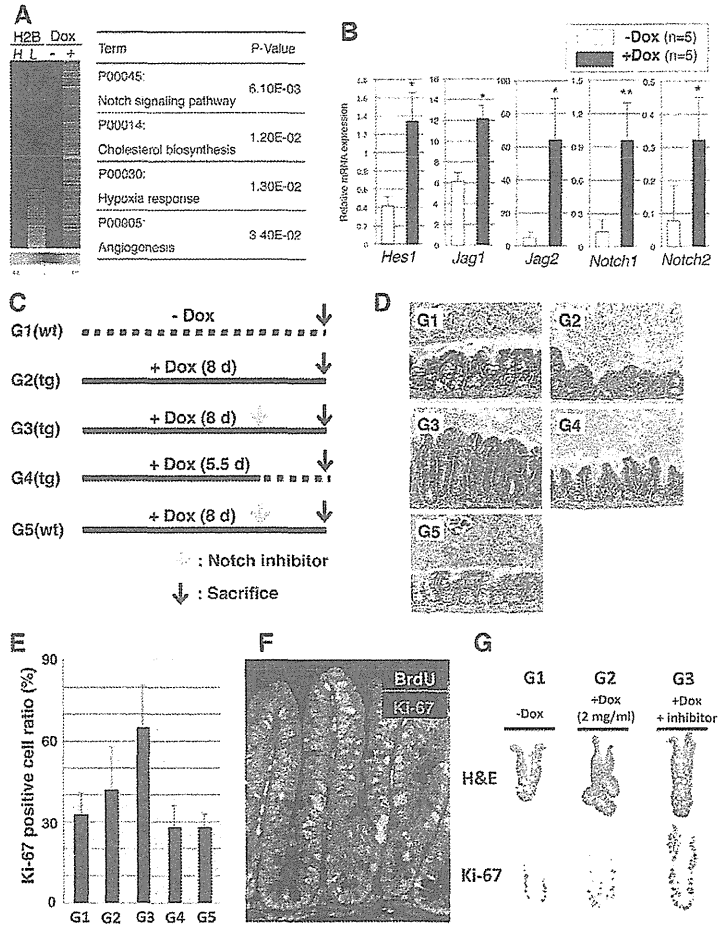

Fig. 4. Notch activation contributes to the maintenance of a slow-cycling state in β-catenin-induced colon. (**A**) Activation of Notch signalling pathway in β-catenin-induced slow-cycling colonic epithelium. Genes specifically upregulated in β-catenin-induced cells, but not in fast-cycling cells (GFP-Low cells in the H2B-GFP experiment) were selected. The heat map shows log2-fold changes in gene expression between β-catenin-induced and non-induced colon (right two columns in the left panel) and between histone-GFP-low and high cells (left two columns). The values for β-catenin non-induced colon and histone-GFP-high cells were used as normalisation for comparison, respectively. Subsequently, gene enrichment analysis were performed using DAVID on the selected genes and revealed that genes in a Notch signalling pathway are significantly concentrated in β-catenin-induced cells. All of the significantly enriched pathways in β-catenin-induced cells are listed in the table. H2B, histone H2B-GFP mouse; H, GFP^{high} cells; L, GFP^{low} cells; Dox, doxycycline treatment for β-catenin induction. (**B**) qRT-PCR analyses of Notch signalling related genes in β-catenin-induce colonic crypts. The Notch target *Hes1*, the Notch ligands *Jag1* and *Jag2*, and the Notch receptors *Notch1* and *Notch2* are strongly upregulated in β-catenin-activated crypts. Data are means ± s.d.; $^{*}P<0.05$, $^{**}P<0.01$, by Mann–Whitney *U*-test. (**C**,**D**) Experimental protocols for treatment with the Notch inhibitor (C) and the representative histology in each group (D). A Notch inhibitor was administrated orally at 2 days prior to sacrifice. (**E**) The Notch inhibitor induces active proliferation in β-catenin-induced colon. Ki-67-positive cell ratio (percentage of Ki-67-positive cells) is significantly higher in G3 than in other groups ($P<0.00001$ for G1, G4 and G5, and $P<0.0005$ for G2, by one-way ANOVA and Turkey's post hoc test, respectively). (**F**) BrdU pulse-chase experiment in mice treated with doxycycline and Notch inhibitor (protocol G3). Double immunostaining for BrdU (green) and Ki-67 (red) on a colon section. The Notch inhibitor reduces BrdU-retention in colonic crypts, whereas it increases Ki-67-positive cells throughout the crypt. (**G**) H&E staining and Ki-67 immunostaining of isolated crypts. The Notch inhibitor induces active cell proliferation and suppressed the *de novo* crypt formation in β-catenin induced crypts.

to the increased number of BrdU-retaining cells following β-catenin induction alone (Fig. 3B), combined treatment with doxycycline and the Notch inhibitor reduced the number of BrdU-retaining nuclei, whereas it increased the number of Ki-67-positive cells (Fig. 4F). These findings suggest that treatment with the Notch inhibitor induces proliferation of slow-cycling cells that have accumulated as a consequence of β-catenin expression. Importantly, treatment of β-catenin-induced mice with the Notch inhibitor also normalised crypt fission and budding rates (Fig. 4G; supplementary material Fig. S8A), which was accompanied by decreased nuclear β-catenin expression without a change in gene expression at the mRNA level (supplementary material Fig. S8B,C). These results indicate that Notch activation contributes to the maintenance of a slow-cycling state and to *de novo* crypt formation in β-catenin-induced colon, and, hence, Notch inhibition turns slow-cycling cells into fast-cycling cells in the context of transgenic β-catenin expression. However, in spite of the clear morphological changes, we could not detect a change in gene expression of the Notch target

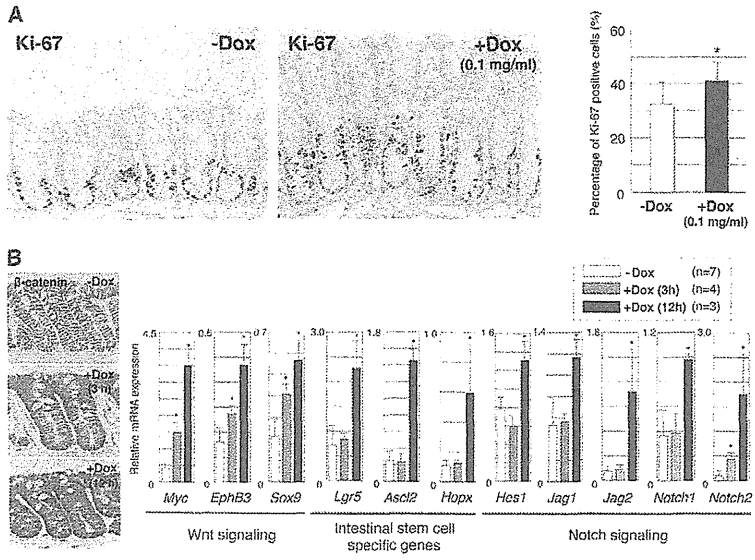

Fig. 5. Dose-dependent effect of Wnt activation on cell proliferation and gene expression in colonic epithelium. (**A**) Lower level of β-catenin induction promotes colonic epithelial proliferation. Ki-67 immunostaining and percentage of Ki-67-positive cells in colonic section from β-catenin-inducible mice treated with lower dose of doxycycline. Lower levels of β-catenin induction increase Ki-67 positive cell ratio and elongate the proliferating compartment of the crypts. Data are mean ± s.d.; **P*<0.05, by Welch's *t*-test. (**B**) Expression of Wnt target genes, ISC-specific genes and Notch signalling-related genes in the colonic crypts with different levels of β-catenin. The different levels of β-catenin accumulation are shown in the left-hand panels. Data are mean ± s.d.; **P*<0.05 compared with non-treated mice, by Kruskal–Wallis test followed by Steel test.

Hes1 in β-catenin-induced mice treated with the Notch inhibitor (data not shown). It is possible that the Notch inhibitor led to a transient inactivation of Notch signalling and thus the altered *Hes1* expression was not detectable at 2 days after treatment. However, given that the Notch/γ-secretase inhibitor has multiple substrates, we cannot completely rule out the possibility that the effect was partly independent of Notch inhibition.

Lower levels of β-catenin activation induce active proliferation of progenitor cells, but not stem cell expansion

In contrast to the well-established role of canonical Wnt signalling in activating cell proliferation in the intestine (Sansom et al., 2004; Andreu et al., 2005), our data show that the Wnt activation confers slow-cycling properties on colonic cells, which is accompanied by *de novo* crypt formation. In an attempt to consolidate these opposing results, we hypothesised that different levels of Wnt signalling may induce different biological outcomes with elevated levels of activation leading to the expansion of slow-cycling ISC-like cells and lower levels of activation inducing active cell proliferation. In order to determine the effects of different levels of β-catenin induction on colon homeostasis, we treated β-catenin-inducible mice with a lower dose of doxycycline than was used previously (0.1 mg/ml in drinking water) and analysed crypt sections. Colonic crypts did not show signs of increased crypt fission/branching rate in mice, suggesting that *de novo* crypt formation is not induced when β-catenin is expressed at low levels (Fig. 5A). However, low levels of β-catenin increased the number of Ki-67-positive cells, and led to an elongation of crypts (Fig. 5A), indicative of enhanced cell proliferation of progenitor cells. These results suggest that different strengths of canonical Wnt signalling result in different transcriptional outputs and, thus, biological effects.

To examine the effects of different levels of Wnt signalling on transcription, we performed gene expression analyses of colonic crypts with high and low levels of β-catenin accumulation. β-Catenin-inducible mice were intragastrically administered doxycycline (100 mg/kg) and sacrificed 3 and 12 hours later, leading to different levels of β-catenin accumulation in the colonic crypts (Fig. 5B). We found that *Myc*, *EphB3* and *Sox9*, well-known targets of canonical Wnt signalling, were upregulated in crypts with both higher and lower levels of β-catenin expression in a level-dependent manner (Fig. 5B). However, activation of the Notch target gene *Hes1* was detected only in crypts with high β-catenin, which is accompanied by the upregulation of ISC-specific genes including *Lgr5*, *Ascl2* and *Hopx* (Fig. 5B). We also examined the gene expression in colonic crypts isolated from β-catenin-inducible mice treated with a lower dose of doxycycline in drinking water (0.1 mg/ml) and found that the lower dose treatment significantly upregulated the expression of Wnt target genes such as *Myc*, but the same treatment did not induce *Lgr5* and *Hes1* in colonic crypts (supplementary material Fig. S9). Together, these results show that activation of the Notch signalling pathway and amplification of ISC-like cells require higher level of β-catenin accumulation. In addition, the expression of the Cdk inhibitors *Cdkn1a*, *Cdkn1b* and *Cdkn1c* were not altered by the lower level of β-catenin induction (supplementary material Fig. S9) in sharp contrast to the case of the higher level of β-catenin induction (supplementary material Fig. S5), suggesting that altered expression of Cdk inhibitors might be responsible for the different proliferative activities.

Colon tumors show heterogeneity in nuclear β-catenin expression and slow-cycling cells in the $Apc^{Min/+}$ mouse model

A large body of evidence indicates that accumulation of β-catenin is an initiating event in intestinal carcinogenesis (Harada et al., 1999; Yamada et al., 2002). The vast majority of colon cancers show accumulation of β-catenin and expression of elevated levels of β-catenin/Tcf target genes. However, strong nuclear accumulation of β-catenin is only observed in a subset of tumour cells, indicating heterogeneity of tumour cells within the tumour (Fodde and Brabletz, 2007). Similarly, we found that colon tumours in $Apc^{Min/+}$ mice, a well-established model for colon tumorigenesis, also show heterogeneous expression of nuclear β-catenin (Fig. 6A). To determine whether such heterogeneous expression of nuclear β-catenin affects downstream transcription of the canonical Wnt signalling, we examined colon tumours of $Apc^{Min/+}$ mice carrying a transgenic GFP reporter allele of β-catenin/Tcf transcription (Oyama et al., 2008). Double

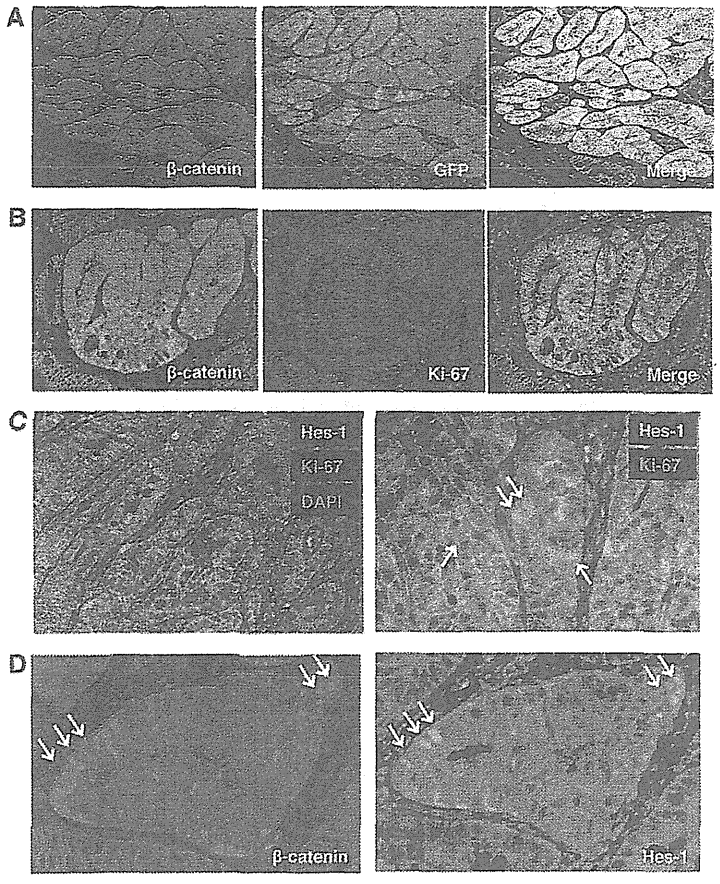

Fig. 6. Heterogeneity of colon tumour cells in *Apc*$^{Min/+}$ mouse. (**A**) Double immunostaining for β-catenin (red) and GFP (green) in the colon tumour of *Apc*$^{Min/+}$ mouse with transgenic GFP reporter allele for β-catenin/Tcf transcription activity. Note that heterogeneous expressions of both β-catenin and GFP are observed in a colon tumour. (**B**) Double immunostaining for β-catenin and Ki-67 in a colon tumour. Tumor cells with strong β-catenin expression show less frequent staining for Ki-67. (**C**) Double immunostaining for Hes1 (green) and Ki-67 (red). Distinct localisation of Hes1-expressing cells and Ki-67-positive cells are seen in colon tumour. Arrows indicate cells with positive nuclear staining for Hes1. (**D**) Immunostaining for β-catenin and Hes1 in serial sections. Colocalisation of higher levels of β-catenin and Hes1 expression is observed in the colon tumour.

immunofluorescence staining revealed that β-catenin levels were well correlated with GFP intensity, demonstrating that different levels of β-catenin accumulation directly affect β-catenin/Tcf transcription in colonic tumours (Fig. 6A). Importantly, most tumour cells with nuclear β-catenin did not express Ki-67 (Fig. 6B), recapitulating our observations in β-catenin-overexpressing mice. When the intensity and localisation of β-catenin expression were examined by immunofluorescence staining, the majority of Ki-67-positive tumour cells showed cytoplasmic β-catenin expression (93.6%) rather than strong nuclear expression (6.4%). In addition to the heterogeneous pattern of nuclear β-catenin accumulation, expression of Hes1 was detectable only in a small subset of colon tumour cells (Fig. 6C,D). Co-staining for Ki-67 revealed that tumour cells with high levels of Hes1 do not divide actively (Fig. 6C). Furthermore, we found that cells with a nuclear β-catenin signal often exhibited high Hes1 expression (Fig. 6D), as we have seen in β-catenin-induced crypts (supplementary material Fig. S4). These findings indicate that colon tumours, like our β-catenin inducible mouse model, consist of heterogeneous populations of cells displaying different activities of canonical Wnt signalling, Notch signalling and cell proliferation.

DISCUSSION

Previous studies using conditional *Apc* knockout mice demonstrated that acute loss of the *Apc* gene rapidly expands progenitor cells in the intestinal crypts (Sansom et al., 2004; Andreu et al., 2005) but does not lead to crypt fission/branching, suggesting that Wnt activation through loss of *Apc* is not sufficient to induce *de novo* crypt formation. In the present study, we showed that high levels of β-catenin activation are sufficient for *de novo* crypt formation of adult mice (Fig. 2). Our observation suggests that β-catenin activation amplifies ISCs, which is consistent with recent work carried out in *Drosophila* hindgut (Takashima et al., 2008). The discrepancy between previous reports and our study seems to arise from differences in the levels of Wnt activation. In fact, by titrating down the levels of activated β-catenin, we also failed to induce *de novo* crypt formation but instead expanded the proliferating progenitor compartment of the crypts (Fig. 5A). These combined findings strongly suggest that high levels of the canonical Wnt effector β-catenin are required for ISC expansion, whereas low levels of activation can induce the active proliferation of progenitor cells. This notion is consistent with a recent finding, which demonstrated that different levels of Wnt signalling exert distinct roles on the self-renewal and differentiation potentials of haematopoietic stem cells (Luis et al., 2011).

The notion that *de novo* crypt formation and cell proliferation are controlled by distinct levels of β-catenin activation is reminiscent of previous observations from our laboratory on the two-stage tumorigenesis of the *Apc*$^{Min/+}$ mouse (Yamada et al., 2002; Oyama et al., 2008). In the colon of *Apc*$^{Min/+}$ mice, we detected many microadenomas as early as 3 weeks of age, of which only a limited number progressed to large tumours. Although early

microadenomas already harboured frequent loss of *Apc* and increased β-catenin/Tcf transcription, larger tumours exhibited further elevations of β-catenin/Tcf transcriptional activity, thus suggesting that increased β-catenin/Tcf signalling is required for the development of larger tumours. The dose-dependent effect of Wnt activation on intestinal tumorigenesis has also been implicated in mouse models with different hypomorphic *Apc* mutant alleles, supporting the requirement for higher levels of Wnt activation for intestinal tumorigenesis (Gaspar and Fodde, 2004). A series of previous studies demonstrated that epigenetic modifications associated with DNA methylation are involved in the transition from microadenomas to large tumours in the $Apc^{Min/+}$ mouse (Yamada et al., 2005; Lin et al., 2006; Linhart et al., 2007). In human colorectal cancers, it has been shown that epigenetic silencing of SFRPs, negative modifiers of Wnt signalling, are frequently found, and such inactivation can further activate the canonical Wnt signals in colon cancer cell lines with *APC* or *CTNNB1* mutations (Suzuki et al., 2004). It is therefore possible that activation of the canonical Wnt signalling by both genetic and epigenetic alterations enables colonic stem cells to expand, leading to *de novo* crypt formation, which ultimately results in tumour growth.

A number of signalling cascades have been implicated in the maintenance of intestinal homeostasis (Scoville et al., 2008), but it remains unclear how the Wnt signalling pathway connects with other signalling cascades within the intestine to control homeostasis. Here, we showed that canonical Wnt signalling plays an important role in *de novo* crypt formation in the colon, and that a higher level of β-catenin activation is crucial for Notch activation. Our finding that Notch inhibition prevented crypt fission/branching in β-catenin-induced colon indicates the requirement for Notch activation in β-catenin-induced *de novo* crypt formation (Fig. 4G; supplementary material Fig. S8A). Interestingly, β-catenin activation rapidly induced transcriptional activation of the Notch ligands *Jag1* and *Jag2*, and the Notch receptors *Notch1* and *Notch2* (Fig. 4B, Fig. 5B), thus offering a possible direct link between these two pathways. Together with previous findings that β-catenin induces *Jag1* transcription, leading to Notch activation in human colon cancer cell lines (Rodilla et al., 2009), it is therefore likely that the increased expression of Notch ligands by β-catenin induction causes Notch activation in the colonic epithelium. Furthermore, a recent study clearly demonstrated that Notch1 and Notch2 receptors are expressed specifically in ISCs (Fre et al., 2011; Sato et al., 2011). The increased expressions of Notch receptors could play a role in the induction of ISC-like cells by β-catenin induction (Fig. 4B). It is also noteworthy that the constitutive activation of Notch results in no obvious effect on β-catenin nuclear localisation (Fre et al., 2005). These findings indicate a hierarchical relationship between the Wnt and Notch signalling pathways in the intestinal epithelium. This hierarchy might explain why genetic alterations in colon cancers are frequently detected in the Wnt signalling pathway, but not in the Notch signalling pathway.

The failure of most current therapies to cure cancer has led to the hypothesis that treatments targeted at malignant proliferation spare a slowly cycling cancer stem cell population. In this study, higher levels of Wnt activation induced *de novo* crypt formation and induced crypt cells to acquire slow-cycling properties. Interestingly, our observation of a β-catenin-induced slow-cycling property is consistent with previous reports in human colorectal cancers. Human colourectal cancers showed heterogeneous intracellular distribution of β-catenin, and tumour cells with nuclear accumulation revealed low cell proliferation rates (Brabletz et al., 2001; Fodde and Brabletz, 2007). Importantly, we also found that colon tumours in $Apc^{Min/+}$ mice consist of heterogeneous cells displaying different levels of β-catenin accumulation and downstream gene expression (Fig. 6A), and tumour cells with nuclear β-catenin are dividing more slowly than surrounding tumour cells, suggesting that such cells are similar to cells at the crypt bottom of the normal colon. Thus, we propose that a hierarchical control of cell proliferation in the colonic crypt epithelium is retained to some extent in colonic neoplasms. Accordingly, we found that tumour cells with nuclear β-catenin are accompanied by high Notch signalling (Fig. 6D), as has been reported in crypt bottom cells (Kayahara et al., 2003). It is interesting to note that a γ-secretase inhibitor turned slow-cycling cells into actively proliferating cells (Fig. 4C-G; supplementary material Fig. S7A). A previous study showed that Notch inhibitors turn undifferentiated, proliferating cells into quiescent cells in colorectal neoplasias (van Es et al., 2005), indicating that the Notch inhibitor might be of therapeutic benefit in colorectal cancers. The discrepancy in the effects of Notch inhibitor could be explained by differences in states of the affected cells between proliferating progenitor cells and ISC-like cells. Although the previous study showed effects on the transition of proliferating cells into terminally differentiated quiescent cells, our data suggest that a Notch inhibitor may promote the transition of slow-cycling ISC-like cells into progenitor cells in the colon. Considering the chemoresistance of slow-cycling cancer stem cells, the results also suggest that Notch inhibitors combined with chemotherapeutic agents and/or irradiation might be effective as treatments targeting slow-cycling cancer stem cells in the colon.

In summary, our results indicate that, although proliferating progenitor cells in colonic crypts physiologically express higher levels of β-catenin/Tcf transcriptions, a further activation of the canonical Wnt singalling leads to *de novo* crypt formation, consisting of relatively slow-cycling cells in the adult colon, which is accompanied by activation of Notch signalling with transactivation of Notch ligands and receptors. However, treatment with a Notch/γ-secretase inhibitor turns such slow-cycling cells into proliferating cells, although we cannot exclude the possibility that some of the observed phenotypes are the result of superphysiological β-catenin expression obtained with our transgenic system. These findings suggest that Wnt and Notch signalling act in a synergistic and hierarchical manner to control differentiation and proliferation of the colonic crypt epithelium *in vivo*.

Acknowledgements
We thank Ayako Suga, Kyoko Takahashi, Huilan Zhi and Yoshitaka Kinjyo for technical assistance, and Hans Clevers for providing the S33 β-catenin overexpression vector.

Funding
This study is supported by PRESTO, Grants-in-Aid from the Ministry of Health, Labour and Welfare of Japan, and Ministry of Education, Culture, Sports, Science and Technology of Japan [Y.Y.]. J.U. is supported by grants of the German Cancer Aid and German Research Council [SFB873]. K.H. was supported by the National Institutes of Health [DP2OD003266 and R01HD058013]. Deposited in PMC for release after 12 months.

Competing interests statement
The authors declare no competing financial interests.

Supplementary material
Supplementary material available online at
http://dev.biologists.org/lookup/suppl/doi:10.1242/dev.084103/-/DC1

References

Andreu, P., Colnot, S., Godard, C., Gad, S., Chafey, P., Niwa-Kawakita, M., Laurent-Puig, P., Kahn, A., Robine, S., Perret, C. et al. (2005). Crypt-restricted proliferation and commitment to the Paneth cell lineage following Apc loss in the mouse intestine. *Development* **132**, 1443-1451.

Barker, N., van Es, J. H., Kuipers, J., Kujala, P., van den Born, M., Cozijnsen, M., Haegebarth, A., Korving, J., Begthel, H., Peters, P. J. et al. (2007). Identification of stem cells in small intestine and colon by marker gene Lgr5. *Nature* **449**, 1003-1007.

Beard, C., Hochedlinger, K., Plath, K., Wutz, A. and Jaenisch, R. (2006). Efficient method to generate single-copy transgenic mice by site-specific integration in embryonic stem cells. *Genesis* **44**, 23-28.

Brabletz, T., Jung, A., Reu, S., Porzner, M., Hlubek, F., Kunz-Schughart, L. A., Knuechel, R. and Kirchner, T. (2001). Variable beta-catenin expression in colorectal cancers indicates tumor progression driven by the tumor environment. *Proc. Natl. Acad. Sci. USA* **98**, 10356-10361.

Fevr, T., Robine, S., Louvard, D. and Huelsken, J. (2007). Wnt/beta-catenin is essential for intestinal homeostasis and maintenance of intestinal stem cells. *Mol. Cell. Biol.* **27**, 7551-7559.

Fodde, R. and Brabletz, T. (2007). Wnt/beta-catenin signaling in cancer stemness and malignant behavior. *Curr. Opin. Cell Biol.* **19**, 150-158.

Foudi, A., Hochedlinger, K., Van Buren, D., Schindler, J. W., Jaenisch, R., Carey, V. and Hock, H. (2009). Analysis of histone 2B-GFP retention reveals slowly cycling hematopoietic stem cells. *Nat. Biotechnol.* **27**, 84-90.

Fre, S., Huyghe, M., Mourikis, P., Robine, S., Louvard, D. and Artavanis-Tsakonas, S. (2005). Notch signals control the fate of immature progenitor cells in the intestine. *Nature* **435**, 964-968.

Fre, S., Hannezo, E., Sale, S., Huyghe, M., Lafkas, D., Kissel, H., Louvi, A., Greve, J., Louvard, D. and Artavanis-Tsakonas, S. (2011). Notch lineages and activity in intestinal stem cells determined by a new set of knock-in mice. *PLoS ONE* **6**, e25785.

Gaspar, C. and Fodde, R. (2004). APC dosage effects in tumorigenesis and stem cell differentiation. *Int. J. Dev. Biol.* **48**, 377-386.

Harada, N., Tamai, Y., Ishikawa, T., Sauer, B., Takaku, K., Oshima, M. and Taketo, M. M. (1999). Intestinal polyposis in mice with a dominant stable mutation of the beta-catenin gene. *EMBO J.* **18**, 5931-5942.

He, X. C., Yin, T., Grindley, J. C., Tian, Q., Sato, T., Tao, W. A., Dirisina, R., Porter-Westpfahl, K. S., Hembree, M., Johnson, T. et al. (2007). PTEN-deficient intestinal stem cells initiate intestinal polyposis. *Nat. Genet.* **39**, 189-198.

Ito, T., Udaka, N., Yazawa, T., Okudela, K., Hayashi, H., Sudo, T., Guillemot, F., Kageyama, R. and Kitamura, H. (2000). Basic helix-loop-helix transcription factors regulate the neuroendocrine differentiation of fetal mouse pulmonary epithelium. *Development* **127**, 3913-3921.

Jung, A., Schrauder, M., Oswald, U., Knoll, C., Sellberg, P., Palmqvist, R., Niedobitek, G., Brabletz, T. and Kirchner, T. (2001). The invasion front of human colorectal adenocarcinomas shows co-localization of nuclear beta-catenin, cyclin D1, and p16INK4A and is a region of low proliferation. *Am. J. Pathol.* **159**, 1613-1617.

Kaneko, Y., Sakakibara, S., Imai, T., Suzuki, A., Nakamura, Y., Sawamoto, K., Ogawa, Y., Toyama, Y., Miyata, T. and Okano, H. (2000). Musashi1: an evolutionally conserved marker for CNS progenitor cells including neural stem cells. *Dev. Neurosci.* **22**, 139-153.

Kayahara, T., Sawada, M., Takaishi, S., Fukui, H., Seno, H., Fukuzawa, H., Suzuki, K., Hiai, H., Kageyama, R., Okano, H. et al. (2003). Candidate markers for stem and early progenitor cells, Musashi-1 and Hes1, are expressed in crypt base columnar cells of mouse small intestine. *FEBS Lett.* **535**, 131-135.

Korinek, V., Barker, N., Moerer, P., van Donselaar, E., Huls, G., Peters, P. J. and Clevers, H. (1998). Depletion of epithelial stem-cell compartments in the small intestine of mice lacking Tcf-4. *Nat. Genet.* **19**, 379-383.

Kuhnert, F., Davis, C. R., Wang, H. T., Chu, P., Lee, M., Yuan, J., Nusse, R. and Kuo, C. J. (2004). Essential requirement for Wnt signaling in proliferation of adult small intestine and colon revealed by adenoviral expression of Dickkopf-1. *Proc. Natl. Acad. Sci. USA* **101**, 266-271.

Li, L. and Clevers, H. (2010). Coexistence of quiescent and active adult stem cells in mammals. *Science* **327**, 542-545.

Lin, H., Yamada, Y., Nguyen, S., Linhart, H., Jackson-Grusby, L., Meissner, A., Meletis, K., Lo, G. and Jaenisch, R. (2006). Suppression of intestinal neoplasia by deletion of Dnmt3b. *Mol. Cell. Biol.* **26**, 2976-2983.

Linhart, H. G., Lin, H., Yamada, Y., Moran, E., Steine, E. J., Gokhale, S., Lo, G., Cantu, E., Ehrich, M., He, T. et al. (2007). Dnmt3b promotes tumorigenesis *in vivo* by gene-specific *de novo* methylation and transcriptional silencing. *Genes Dev.* **21**, 3110-3122.

Luis, T. C., Naber, B. A., Roozen, P. P., Brugman, M. H., de Haas, E. F., Ghazvini, M., Fibbe, W. E., van Dongen, J. J., Fodde, R. and Staal, F. J. (2011). Canonical wnt signaling regulates hematopoiesis in a dosage-dependent fashion. *Cell Stem Cell* **9**, 345-356.

Morin, P. J., Sparks, A. B., Korinek, V., Barker, N., Clevers, H., Vogelstein, B. and Kinzler, K. W. (1997). Activation of beta-catenin-Tcf signaling in colon cancer by mutations in beta-catenin or AP. *Science* **275**, 1787-1790.

Oyama, T., Yamada, Y., Hata, K., Tomita, H., Hirata, A., Sheng, H., Hara, A., Aoki, H., Kunisada, T., Yamashita, S. et al. (2008). Further upregulation of beta-catenin/Tcf transcription is involved in the development of macroscopic tumors in the colon of ApcMin/+ mice. *Carcinogenesis* **29**, 666-672.

Pinto, D., Gregorieff, A., Begthel, H. and Clevers, H. (2003). Canonical Wnt signals are essential for homeostasis of the intestinal epithelium. *Genes Dev.* **17**, 1709-1713.

Potten, C. S., Booth, C., Tudor, G. L., Booth, D., Brady, G., Hurley, P., Ashton, G., Clarke, R., Sakakibara, S. and Okano, H. (2003). Identification of a putative intestinal stem cell and early lineage marker; musashi-1. *Differentiation* **71**, 28-41.

Rodilla, V., Villanueva, A., Obrador-Hevia, A., Robert-Moreno, A., Fernández-Majada, V., Grilli, A., López-Bigas, N., Bellora, N., Albà, M. M., Torres, F. et al. (2009). Jagged1 is the pathological link between Wnt and Notch pathways in colorectal cancer. *Proc. Natl. Acad. Sci. USA* **106**, 6315-6320.

Sangiorgi, E. and Capecchi, M. R. (2008). Bmi1 is expressed *in vivo* in intestinal stem cells. *Nat. Genet.* **40**, 915-920.

Sansom, O. J., Reed, K. R., Hayes, A. J., Ireland, H., Brinkmann, H., Newton, I. P., Batlle, E., Simon-Assmann, P., Clevers, H., Nathke, I. S. et al. (2004). Loss of Apc *in vivo* immediately perturbs Wnt signaling, differentiation, and migration. *Genes Dev.* **18**, 1385-1390.

Sato, T., van Es, J. H., Snippert, H. J., Stange, D. E., Vries, R. G., van den Born, M., Barker, N., Shroyer, N. F., van de Wetering, M. and Clevers, H. (2011). Paneth cells constitute the niche for Lgr5 stem cells in intestinal crypts. *Nature* **469**, 415-418.

Scoville, D. H., Sato, T., He, X. C. and Li, L. (2008). Current view: intestinal stem cells and signaling. *Gastroenterology* **134**, 849-864.

Suzuki, H., Watkins, D. N., Jair, K. W., Schuebel, K. E., Markowitz, S. D., Chen, W. D., Pretlow, T. P., Yang, B., Akiyama, Y., Van Engeland, M. et al. (2004). Epigenetic inactivation of SFRP genes allows constitutive WNT signaling in colorectal cancer. *Nat. Genet.* **36**, 417-422.

Takashima, S., Mkrtchyan, M., Younossi-Hartenstein, A., Merriam, J. R. and Hartenstein, V. (2008). The behaviour of Drosophila adult hindgut stem cells is controlled by Wnt and Hh signalling. *Nature* **454**, 651-655.

Takeda, N., Jain, R., LeBoeuf, M. R., Wang, Q., Lu, M. M. and Epstein, J. A. (2011). Interconversion between intestinal stem cell populations in distinct niches. *Science* **334**, 1420-1424.

Tsukamoto, T., Fukami, H., Yamanaka, S., Yamaguchi, A., Nakanishi, H., Sakai, H., Aoki, I. and Tatematsu, M. (2001). Hexosaminidase-altered aberrant crypts, carrying decreased hexosaminidase alpha and beta subunit mRNAs, in colon of 1,2-dimethylhydrazine-treated rats. *Jpn. J. Cancer Res.* **92**, 109-118.

Tumbar, T., Guasch, G., Greco, V., Blanpain, C., Lowry, W. E., Rendl, M. and Fuchs, E. (2004). Defining the epithelial stem cell niche in skin. *Science* **303**, 359-363.

van de Wetering, M., Sancho, E., Verweij, C., de Lau, W., Oving, I., Hurlstone, A., van der Horn, K., Batlle, E., Coudreuse, D., Haramis, A. P. et al. (2002). The beta-catenin/TCF-4 complex imposes a crypt progenitor phenotype on colorectal cancer cells. *Cell* **111**, 241-250.

van der Flier, L. G., Sabates-Bellver, J., Oving, I., Haegebarth, A., De Palo, M., Anti, M., Van Gijn, M. E., Suijkerbuijk, S., Van de Wetering, M., Marra, G. et al. (2007). The Intestinal Wnt/TCF Signature. *Gastroenterology* **132**, 628-632.

van der Flier, L. G., van Gijn, M. E., Hatzis, P., Kujala, P., Haegebarth, A., Stange, D. E., Begthel, H., van den Born, M., Guryev, V., Oving, I. et al. (2009). Transcription factor achaete scute-like 2 controls intestinal stem cell fate. *Cell* **136**, 903-912.

van Es, J. H., van Gijn, M. E., Riccio, O., van den Born, M., Vooijs, M., Begthel, H., Cozijnsen, M., Robine, S., Winton, D. J., Radtke, F. et al. (2005). Notch/gamma-secretase inhibition turns proliferative cells in intestinal crypts and adenomas into goblet cells. *Nature* **435**, 959-963.

van Noort, M., van de Wetering, M. and Clevers, H. (2002). Identification of two novel regulated serines in the N terminus of beta-catenin. *Exp. Cell Res.* 276, 264-272.

Vermeulen, L., De Sousa E Melo, F., van der Heijden, M., Cameron, K., de Jong, J. H., Borovski, T., Tuynman, J. B., Todaro, M., Merz, C., Rodermond, H. et al. (2010). Wnt activity defines colon cancer stem cells and is regulated by the microenvironment. *Nat. Cell Biol.* **12**, 468-476.

Yamada, Y., Hata, K., Hirose, Y., Hara, A., Sugie, S., Kuno, T., Yoshimi, N., Tanaka, T. and Mori, H. (2002). Microadenomatous lesions involving loss of Apc heterozygosity in the colon of adult Apc(Min/+) mice. *Cancer Res.* **62**, 6367-6370.

Yamada, Y., Jackson-Grusby, L., Linhart, H., Meissner, A., Eden, A., Lin, H. and Jaenisch, R. (2005). Opposing effects of DNA hypomethylation on intestinal and liver carcinogenesis. *Proc. Natl. Acad. Sci. USA* **102**, 13580-13585.

Yamashita, S., Nomoto, T., Ohta, T., Ohki, M., Sugimura, T. and Ushijima, T. (2003). Differential expression of genes related to levels of mucosal cell proliferation among multiple rat strains by using oligonucleotide microarrays. *Mamm. Genome* **14**, 845-852.

EWS/ATF1 expression induces sarcomas from neural crest–derived cells in mice

Kazunari Yamada,[1,2] Takatoshi Ohno,[1] Hitomi Aoki,[3] Katsunori Semi,[4,5] Akira Watanabe,[4,5] Hiroshi Moritake,[6] Shunichi Shiozawa,[7] Takahiro Kunisada,[3] Yukiko Kobayashi,[8] Junya Toguchida,[4,8,9] Katsuji Shimizu,[1] Akira Hara,[2] and Yasuhiro Yamada[2,4,5]

[1]Department of Orthopedic Surgery, [2]Department of Tumor Pathology, and [3]Department of Tissue and Organ Development Regeneration and Advanced Medical Science, Gifu University Graduate School of Medicine, Gifu, Japan.
[4]Center for iPS Cell Research and Application (CiRA) and [5]Institute for Integrated Cell-Material Sciences, (WPI-iCeMS), Kyoto University, Kyoto, Japan.
[6]Division of Pediatrics, Department of Reproductive and Developmental Medicine, Faculty of Medicine, University of Miyazaki, Miyazaki, Japan.
[7]Department of Medicine, Kyushu University Beppu Hospital, Beppu, Japan. [8]Department of Tissue Regeneration, Institute for Frontier Medical Sciences, and [9]Department of Orthopaedic Surgery, Kyoto University, Kyoto, Japan.

Clear cell sarcoma (CCS) is an aggressive soft tissue malignant tumor characterized by a unique t(12;22) translocation that leads to the expression of a chimeric *EWS/ATF1* fusion gene. However, little is known about the mechanisms underlying the involvement of *EWS/ATF1* in CCS development. In addition, the cellular origins of CCS have not been determined. Here, we generated *EWS/ATF1*-inducible mice and examined the effects of *EWS/ATF1* expression in adult somatic cells. We found that forced expression of *EWS/ATF1* resulted in the development of *EWS/ATF1*-dependent sarcomas in mice. The histology of *EWS/ATF1*-induced sarcomas resembled that of CCS, and *EWS/ATF1*-induced tumor cells expressed CCS markers, including S100, SOX10, and MITF. Lineage-tracing experiments indicated that neural crest–derived cells were subject to *EWS/ATF1*-driven transformation. EWS/ATF1 directly induced Fos in an ERK-independent manner. Treatment of human and *EWS/ATF1*-induced CCS tumor cells with FOS-targeted siRNA attenuated proliferation. These findings demonstrated that FOS mediates the growth of *EWS/ATF1*-associated sarcomas and suggest that FOS is a potential therapeutic target in human CCS.

Introduction

Clear cell sarcoma (CCS) is an aggressive malignancy of adolescents and young adults that was first described by Enzinger (1). It typically arises in the deep soft tissues of the lower extremities closed to tendon, fascia, and aponeurosis (2). Chemotherapy and radiotherapy are not of any benefit (3–5), and a high rate of local and distant recurrence results in poor survival rates (3, 6, 7). CCSs harbor the potential for melanocytic differentiation and melanin synthesis (8). Gene expression profiles support the classification of CCS as a distinct genomic subtype of melanomas (9). These melanocytic features often make the distinction from malignant melanoma (MM) difficult. However, in contrast to MM, CCS is characterized by a chromosomal translocation, t(12;22)(q13;q12), that leads to the fusion of activating transcription factor 1 (*ATF1*) gene localized to 12q13 to Ewing's sarcoma oncogene (*EWS*) gene at 22q12 in up to 90% of cases, resulting in expression of the *EWS/ATF1* fusion gene (10–12). Given that CCS and MM have such similar characteristics, it has been proposed that CCSs may arise from a neural crest progenitor. However, the exact origin of CCS still remains to be determined.

The biological role of the EWS/ATF1 fusion protein is still unclear. EWS contains a transcriptional activation domain in the N-terminal region (13–15) and several conserved RNA binding motifs in the C-terminal region (16). Binding of the N-terminal region of EWS to the RNA polymerase II subunit hsRPB7 has been proposed to be important for transactivation of the target genes (17). In contrast, ATF1 is a member of the CREB transcription factor family, whose activity is regulated through phosphorylation of its kinase inducible domain (KID) by protein kinase A (18). ATF1 mediates the activation of cAMP-responsive genes through binding to a conserved cAMP-responsive element (CRE) as a dimmer (19, 20). However, the N-terminal activation domain of EWS replaces the KID in the EWS/ATF1 fusion protein, rendering it unable to support a typical inductive signal (21). Therefore, EWS/ATF1 can act as constitutive transcriptional activator in a cAMP-independent fashion with normal CRE DNA binding activity (14, 22, 23).

Previous studies have revealed some target genes of EWS/ATF1, but their true function in tumorigenesis is still not well understood (24). Expression of *MITF* is constitutively activated by *EWS/ATF1* in CCS in vitro (25). Consistent with this finding, several studies have identified the expression of MITF protein or mRNA in CCS (26–28). MITF is a master regulator of melanocyte development and plays a role in melanoma development (29, 30). Importantly, activation of MITF by EWS/ATF1 is required for CCS proliferation as well as for melanocytic differentiation of CCS in vitro (25).

Although previous studies have demonstrated that EWS/ATF1 is associated with oncogenic potential in CCS, the effect of in vivo expression of *EWS/ATF1* on sarcoma formation is still not known. In the present study, we established *EWS/ATF1* transgenic mice using a doxycycline-dependent expression system in order to investigate the role of *EWS/ATF1* on CCS development in vivo. Our results showed that forced expression of *EWS/ATF1* induced CCS-like sarcoma in the transgenic mice. This mouse model was used to identify the origin of *EWS/ATF1*-induced sarcomas as well as the direct target of EWS/ATF1 in these sarcomas.

Results

Inducible expression of EWS/ATF1 in mice. We first generated doxycycline-inducible *EWS/ATF1* ES cells, in which the human *EWS/ATF1* type 2 fusion gene (26, 31) can be induced under the control of

Conflict of interest: The authors have declared that no conflict of interest exists.
Citation for this article: *J Clin Invest.* doi:10.1172/JCI63572.

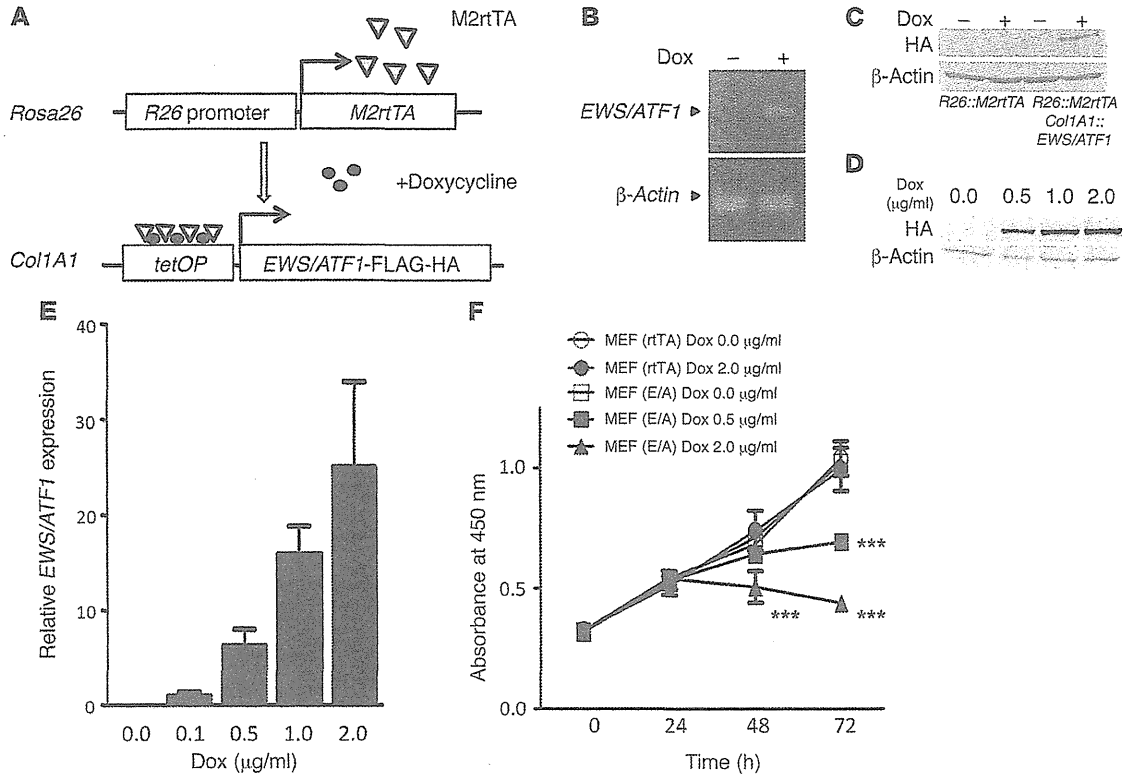

Figure 1

Inducible expression of *EWS/ATF1*. (**A**) Schematic of the doxycycline-inducible *EWS/ATF1* alleles. (**B**) *EWS/ATF1* expression in ES cells, detected by RT-PCR, after exposure to doxycycline for 12 hours. (**C**) EWS/ATF1 expression in ES cells, detected by Western blot, after exposure to doxycycline for 24 hours. (**D**) Dose-dependent induction of EWS/ATF1 protein in *EWS/ATF1*-inducible ES cells by doxycycline. ES cells were exposed to doxycycline concentrations up to 2 μg/ml for 24 hours. Western blot analysis was performed using an anti-HA antibody. (**E**) Dose-dependent doxycycline induction of *EWS/ATF1* mRNA in *EWS/ATF1*-inducible MEFs. MEFs were exposed to different concentrations of doxycycline for 24 hours. Transcript levels were normalized to β-*actin*. Data are mean ± SD ($n = 3$). (**F**) *EWS/ATF1* expression suppressed MEF growth. Cell viability was determined by WST-8 assay. Data are mean ± SD ($n = 4$). Control MEFs (rtTA) and *EWS/ATF1*-inducible MEFs (E/A) were derived from heterozygous *Rosa26::M2rtTA* and *Col1A1::tetO-EWS/ATF1* mice, respectively. ***$P < 0.001$ vs. MEF (rtTA) Dox 0.0 μg/ml, MEF (rtTA) Dox 2.0 μg/ml, and MEF (E/A) Dox 0.0 μg/ml.

a tetracycline-responsive regulatory element (Figure 1A). Upon treatment of these ES cells with doxycycline, expression of the *EWS/ATF1* fusion transcript was detected by RT-PCR (Figure 1B). We also confirmed the expression of EWS/ATF1 protein upon doxycycline treatment (Figure 1C), which was regulated in a dose-dependent manner (up to 2 μg/ml; Figure 1D).

Heterozygous *Rosa26::M2rtTA* mice with heterozygous *tetO-EWS/ATF1* allele were used to induce the *EWS/ATF1* fusion gene. Cultured murine embryonic fibroblasts (MEFs) derived from *EWS/ATF1*-inducible mice were first exposed to doxycycline to test the effect of *EWS/ATF1* expression on somatic cells. *EWS/ATF1* expression at the mRNA level was confirmed 24 hours after exposure (Figure 1E). Unexpectedly, the cell proliferation rate of MEFs decreased after *EWS/ATF1* induction in a doxycycline dose–dependent manner (Figure 1F).

EWS/ATF1 induces sarcoma formation in mice. To investigate the effect of *EWS/ATF1* expression in vivo, we treated *EWS/ATF1*-inducible mice at 6 weeks of age with doxycycline in the drinking water (50 μg/ml). The *EWS/ATF1*-inducible mice given doxycycline started to develop multiple macroscopic soft tissue tumors after 4 weeks. After doxycycline treatment, EWS/ATF1 protein was detected in a variety of tissues, including the intestine, liver, epidermis, and deep soft tissue (Supplemental Figure 1A; supplemental material available online with this article; doi:10.1172/JCI63572DS1). Doxycycline treatment for 3 months resulted in tumor formation in the deep soft tissues of all mice ($n = 39$), whereas control mice without doxycycline treatment developed no detectable tumors. *EWS/ATF1*-induced tumors typically arose in the trunks, heads, limbs, and whisker pads (Figure 2A). Macroscopically, tumors consisted of circumscribed and lobulated gray-white mass (Figure 2A). In most cases, the tumors were attached to fascia or aponeuroses (Figure 2, A and B), which indicates that the tumors specifically arose from the deep soft tissues. Importantly, 36 of 39 mice (92%) developed tumors in the trunk, which suggests that cells located in the trunk are particularly permissive for tumorigenesis by *EWS/ATF1* expression. Despite expression of EWS/ATF1 protein, no tumor formation was observed in other tissues, such as the epidermis and intestine, even in mice given doxycycline for 3 months.

Microscopic examination of these tumors revealed striking similarities to human CCSs. The tumors showed a rather uniform pattern of compact nests or fascicles of rounded or fusiform cells, which were divided by a framework of fibrocollagenous tissue (Figure 2B).

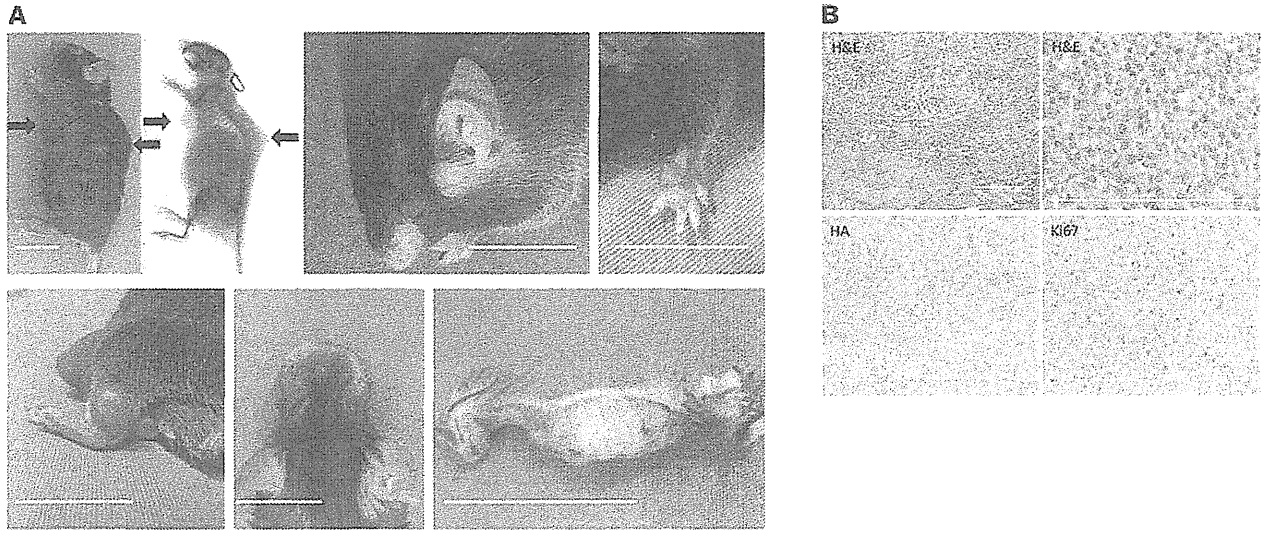

Figure 2
EWS/ATF1-induced tumors resemble human CCS. *EWS/ATF1* transgenic mice were administered 50 μg/ml doxycycline in their drinking water for 3 months. (**A**) *EWS/ATF1* expression caused tumor formation (arrows) in various locations: trunk, head, limbs, and whisker pads. X-ray examination revealed multiple tumors in deep soft tissue. The cut surface of a large tumor on the ventral trunk of an *EWS/ATF1*-inducible mouse revealed a lobulated gray-white mass in the deep soft tissue. Scale bars: 20 mm. (**B**) Histological analysis of *EWS/ATF1*-induced tumors. Tumors were composed of round or fusiform cells with prominent basophilic nuclei and clear cytoplasm, which were surrounded by fibrous fascicles. HA immunostaining confirmed EWS/ATF1 expression in the tumor cells. Frequent Ki67-positive cells were present throughout the lesions. Scale bars: 200 μm (H&E, left); 50 μm (H&E, right); 100 μm (HA and Ki67).

The individual tumor cells had a homogeneous appearance. They had round to ovoid vesicular nuclei with prominent basophilic nucleoli and clear or pale-staining cytoplasm (Figure 2B). The majority of the tumor cells expressed EWS/ATF1 fusion protein in nuclei (Figure 2B and Supplemental Figure 2A). Ki67-positive proliferating cells were observed in about 30%–40% of tumor cells (Figure 2B), indicative of active proliferative activity. The survival curves of *EWS/ATF1*-induced mice were analyzed to evaluate the overall effect of *EWS/ATF1* expression on life span. The transgenic mice treated with doxycycline became moribund within 3–10 months, suggestive of multiple tumor formation in the deep soft tissue, whereas mice without doxycycline treatment survived much longer, and no tumor formation was observed. The median survival time of *EWS/ATF1*-inducible mice treated with doxycycline was 20 weeks (Supplemental Figure 2B).

Previous studies demonstrated that human CCSs express markers for neural crest lineage as well as melanocytic differentiation (8, 9). Therefore, to examine the similarity of mouse *EWS/ATF1*-induced tumors with human CCSs, we performed immunohistochemical analysis for CCS-expressing markers; *EWS/ATF1*-induced tumor cells showed the expression such markers, including S100, Sox10, and Mitf (Figure 3A).

Neural crest–lineage cells are permissive to EWS/ATF1-driven sarcoma development. The cell of origin for CCS remains to be determined. Based on the potential of CCSs for melanocytic differentiation and melanin synthesis, previous studies proposed that CCS may arise from a neural crest progenitor. To determine whether *EWS/ATF1*-induced sarcomas actually arise from neural crest–derived cells, we performed a lineage-tracing experiment in which neural crest–derived cells were tagged by reporter in vivo (32). To label neural crest–derived cells in vivo, we first used transgenic mice containing *Wnt1-Cre* and floxed *LacZ* reporter alleles. We further introduced doxycycline-inducible *EWS/ATF1* alleles into the reporter mice to generate compound transgenic mice (Figure 3B). We confirmed that *EWS/ATF1*-induced tumor cells did not express *Wnt1* (Supplemental Figure 3A). Transgenic mice were treated with doxycycline in the drinking water to induce subcutaneous tumors and the developed tumors were then analyzed for the expression of the reporter gene. Importantly, all 14 *EWS/ATF1*-induced tumors were ubiquitously positive for X-gal staining (Figure 3C and Supplemental Figure 3D), which suggests that neural crest–lineage cells are a cell of origin for *EWS/ATF1*-associated sarcomas. We further performed another lineage-tracing experiment using transgenic mice containing *P0-Cre* and floxed *EYFP* reporter alleles (Figure 3D), which have been also widely used to label neural crest–derived cells. Again, we found that all 6 *EWS/ATF1*-induced tumors were positive for EYFP (Figure 3E and Supplemental Figure 4, C and D).

Establishment of tumor cell lines. Tumor samples were obtained from primary tumors of *EWS/ATF1*-induced mice to establish cell lines from *EWS/ATF1*-induced tumors. We established 2 tumor cell lines, G1297 and G1169, from 2 independent mice. These cells grew in the form of an adherent monolayer in the presence of doxycycline (0.2 μg/ml). We cultured the cells up to the fourth passage in medium containing 0.2 μg/ml doxycycline in order to avoid contamination by fibroblasts. We examined the effect of different concentrations of doxycycline on the growth and morphology of the established cell lines. We confirmed that the expression of *EWS/ATF1* transcript and protein increased in response to doxycycline in a dose-dependent manner in both established cell lines (Supplemental Figure 5, A–C). The growth and morphology of the tumor cells varied in a doxycycline dose–dependent manner: small, round tumor cells grew rapidly at concentrations above 0.1 μg/ml,

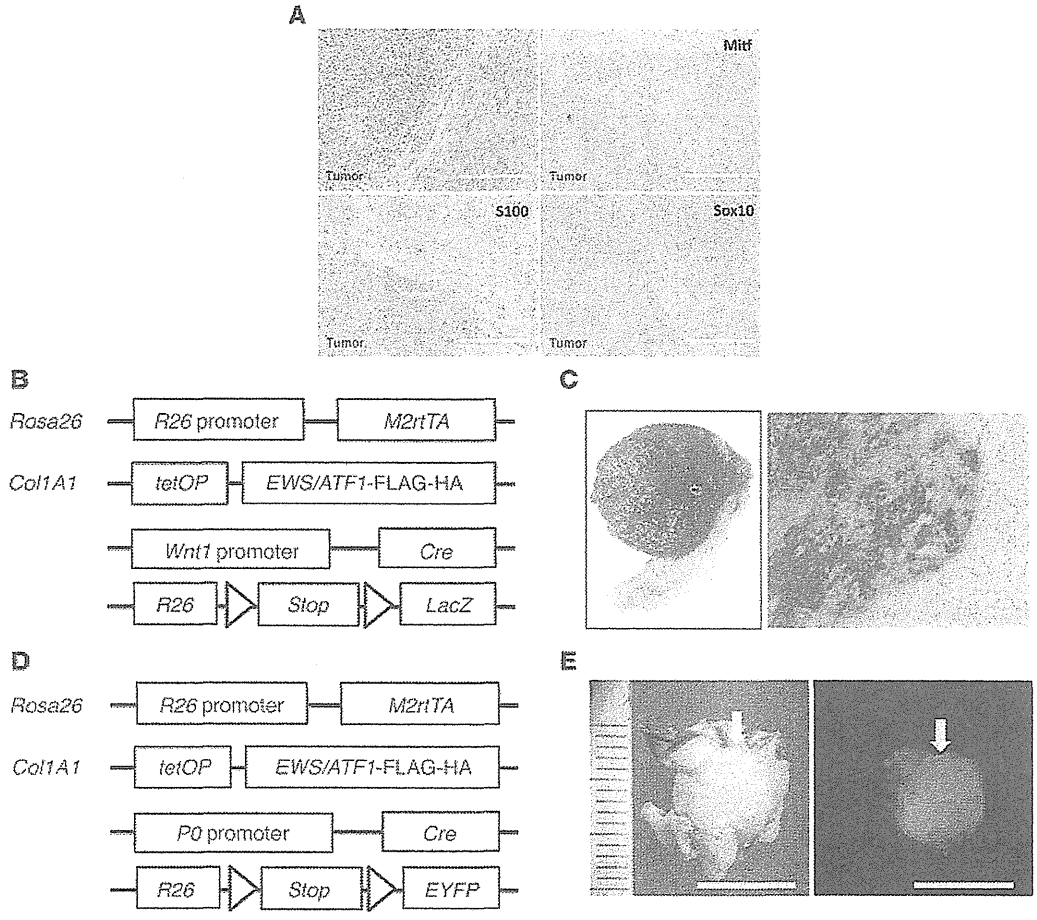

Figure 3

EWS/ATF1-induced tumors arise from neural crest–lineage cells. (**A**) Immunohistochemical analysis for CCS markers. Nuclear staining for S100, Sox10, and Mitf was observed in tumor cells. Sections were counterstained with hematoxylin. Scale bars: 100 μm. (**B**) Schematic representation of reporter alleles for the lineage-tracing experiment using *Wnt1-Cre* allele. Doxycycline-inducible *EWS/ATF1* alleles were introduced into reporter mice containing the *Wnt1-Cre* and floxed *LacZ* reporter alleles. (**C**) X-gal staining for *EWS/ATF1*-induced tumors with *Wnt1-Cre* and floxed *LacZ* reporter alleles. Positive staining for X-gal indicated that the tumor arose from a neural crest–lineage cell. Histological analysis revealed that neoplastic cells were stained with X-gal. Counterstaining was performed with fast red. Scale bars: 2 mm (left); 50 μm (right). (**D**) Schematic representation of reporter alleles for the lineage-tracing experiment using *P0-Cre* allele. Doxycycline-inducible *EWS/ATF1* alleles were introduced into reporter mice containing the *P0-Cre* and floxed *EYFP* reporter alleles. (**E**) Representative image of a tumor (arrow) in the trunk of an *EWS/ATF1*-induced mouse with *P0-Cre* and floxed *EYFP* reporter alleles. Fluorescent signals for EYFP expression were detected in the. Scale bars: 10 mm.

whereas dendritic fibroblast–like spindle cells were observed below 0.05 μg/ml (Figure 4A). Notably, doxycycline withdrawal caused rapid morphological changes, into a fibroblast-like shape, and these tumor cells did not proliferate up to the next passage (Figure 4A). Consistent with these findings, cell viability assay revealed that the number of cells was increased by doxycycline treatment in a dose-dependent manner (Figure 4B). We next examined the effect of *EWS/ATF1* expression on tumorigenesis ability in the subcutaneous tissue of immunocompromised mice. The established cell line G1297 was cultured in medium containing 0.2 μg/ml doxycycline, and 5.0×10^6 cells were transplanted into the subcutaneous tissue of nude mice. It is important to note that all mice treated with 50 μg/ml doxycycline in the drinking water developed tumors within 3 weeks, whereas no tumor formation was observed in mice without doxycycline treatment (Figure 4C). Histological analysis revealed that the subcutaneous tumors in nude mice consisted of neoplastic cells that resembled the primary tumor cells in *EWS/ATF1*-induced transgenic mice (Figure 4D). Positive immunoreactivity for HA-Tag was observed in all tumor cells (Figure 4D).

Continuous expression of EWS/ATF1 is required for tumor growth maintenance. To further examine whether continuous expression of *EWS/ATF1* is necessary for the growth of *EWS/ATF1*-induced tumors, we withdrew doxycycline in tumor-bearing EWS/ATF1 transgenic mice that had been given doxycycline for 3 months. Importantly, doxycycline withdrawal resulted in a rapid reduction of tumor mass in 4 independent mice (7 tumors total). The regressed tumors contained fibrous tissue, but no viable neoplastic cells were observed 3 months after doxycycline withdrawal (Figure 4E), which suggests that *EWS/ATF1*-induced tumor growth depends on continuous *EWS/ATF1* expression. We next examined the histological changes shortly after doxycycline withdrawal in order to investigate the mechanisms of tumor regression.

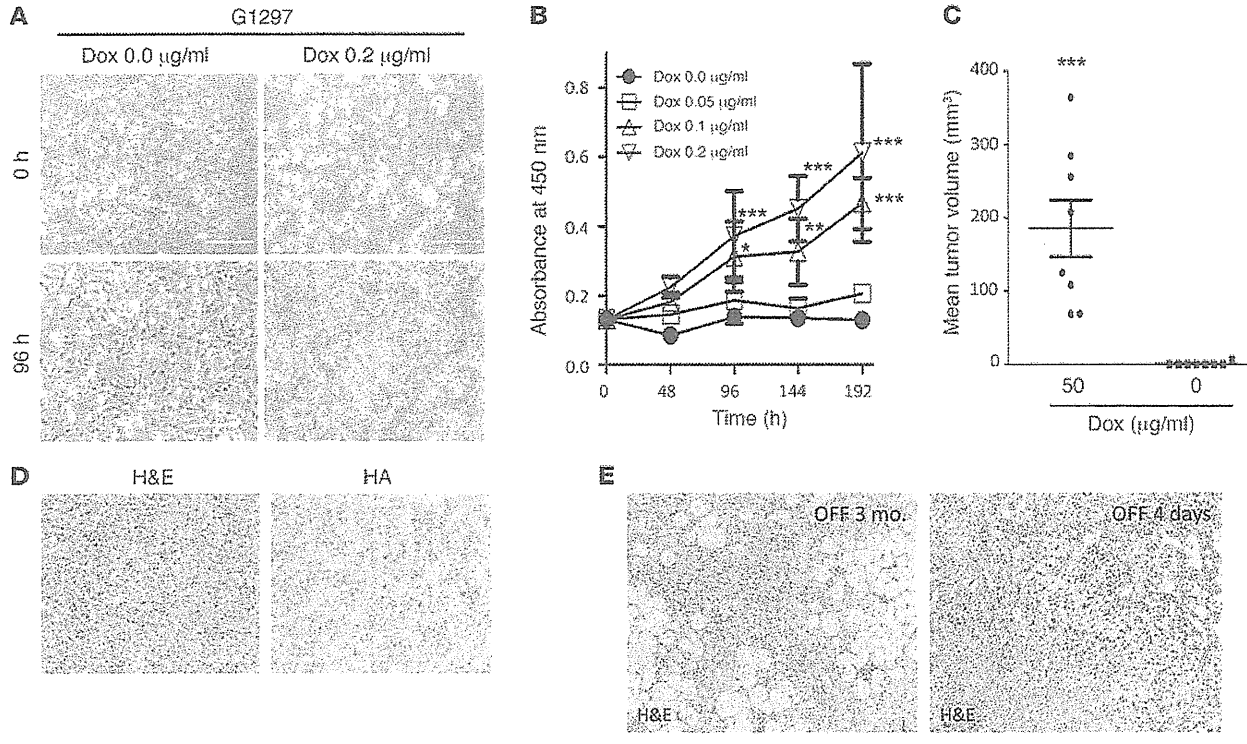

Figure 4

Establishment and analysis of tumor cell lines. G1297 and G1169 cell lines were established from 2 independent *EWS/ATF1*-induced tumors. (**A**) Morphology of the G1297 line after treatment without or with doxycycline (0 and 0.2 μg/ml, respectively). At concentrations above 0.1 μg/ml, small, round tumor cells grew rapidly, while dendritic fibroblast-like spindle cells were observed; tumor cell growth almost stopped at concentrations less than 0.05 μg/ml. Scale bars: 50 μm. (**B**) Effect of different levels of *EWS/ATF1* on tumor cell growth. G1297 cells were cultured in different concentrations of doxycycline (0, 0.05, 0.1, and 0.2 μg/ml), and cell viability was determined by WST-8 assay. Data are mean ± SD ($n = 8$). $^*P < 0.05$, $^{**}P < 0.01$, $^{***}P < 0.001$ vs. Dox 0.0 μg/ml. (**C**) Subcutaneous transplantation of 5.0×10^6 G1297 cells in immunocompromised mice resulted in tumor formation in mice treated with 50 μg/ml doxycycline ($n = 8$). Mean tumor volumes ± SEM are shown. $^{***}P < 0.005$. (**D**) Representative histology and HA immunostaining of tumors in nude mice. The tumor resembled the original sarcoma with EWS/ATF1 expression. Scale bars: 100 μm. (**E**) Doxycycline withdrawal led to rapid tumor regression. At 3 months after doxycycline withdrawal, no viable tumor cells were observed, and tumors were replaced by fibrous tissue. Widespread cell death was observed 4 days after doxycycline withdrawal. Scale bars: 200 μm.

We found widespread cell death within the tumor mass, accompanied by massive infiltration of inflammatory cells, at 4 days after doxycycline withdrawal (Figure 4E), which indicates that neoplastic cells cannot survive in vivo without *EWS/ATF1* expression. Taken together, these results clearly indicate that *EWS/ATF1* plays a pivotal role in the proliferation and maintenance of *EWS/ATF1*-induced tumor cells in vivo.

Fos is a direct target of EWS/ATF1. To determine the downstream targets regulated by EWS/ATF1, we next performed gene expression analysis using G1297 cells. First, we confirmed that withdrawal of doxycycline for 96 hours resulted in no detectable expression of *EWS/ATF1* RNA or protein in cultured tumor cells. Next, the tumor cells were exposed again to doxycycline at a concentration of 0.05 or 0.2 μg/ml, and microarray analysis was performed at 3 and 48 hours after doxycycline exposure. Induction of *EWS/ATF1* resulted in altered expression of a number of genes associated with cell growth, such as growth factor genes (*Areg* and *Ereg*), cell cycle regulators (*Cenpa*, *Ccna2*, *Ccnb2*, *Cdkn1b*, *Plk1*, and *Aurka*), and a proto-oncogene (*Fos*) at either time point (Supplemental Figure 6A). Although a previous study demonstrated that *MITF-M* is a direct target of EWS/ATF1 in human CCS cell lines (25), we failed to detect its expression in our *EWS/ATF1*-induced tumor cell lines and primary tumor samples (Supplemental Figure 7, A and B). Among the transcripts upregulated by *EWS/ATF1*, we focused on the proto-oncogene *Fos*, because this was one of the most highly upregulated genes by *EWS/ATF1* after doxycycline exposure in the microarray analysis (Supplemental Figure 6A). Quantitative real-time RT-PCR (qRT-PCR) confirmed upregulation of both *Fos* and *EWS/ATF1* transgenes in 2 independent tumor cell lines as early as 3 hours after doxycycline exposure (Figure 5A and Supplemental Figure 7C). We also found that the *EWS/ATF1*-induced tumor specimens expressed higher levels of both *Fos* and *EWS/ATF1* transgenes (Figure 5B). Expression of *Fos* is induced by numerous stimuli, which are transmitted through the RAS/Raf/MAP kinase or cAMP-dependent protein kinase pathway (33). In order to investigate the mechanism of *Fos* induction by *EWS/ATF1*, we next examined whether the RAS/Raf/MAP kinase pathway is involved in *EWS/ATF1*-mediated *Fos* activation. In contrast to the rapid and transient induction of Fos in MEFs after serum stimulation (Supplemental Figure 7D), expression of Fos in the *EWS/ATF1*-expressing tumor cell line was detected even under serum-free conditions, and it gradually increased after serum stimulation (Supplemental Figure 7E). Interestingly, whereas serum-stimulated MEFs revealed immediate phosphorylation of ERK1 and ERK2

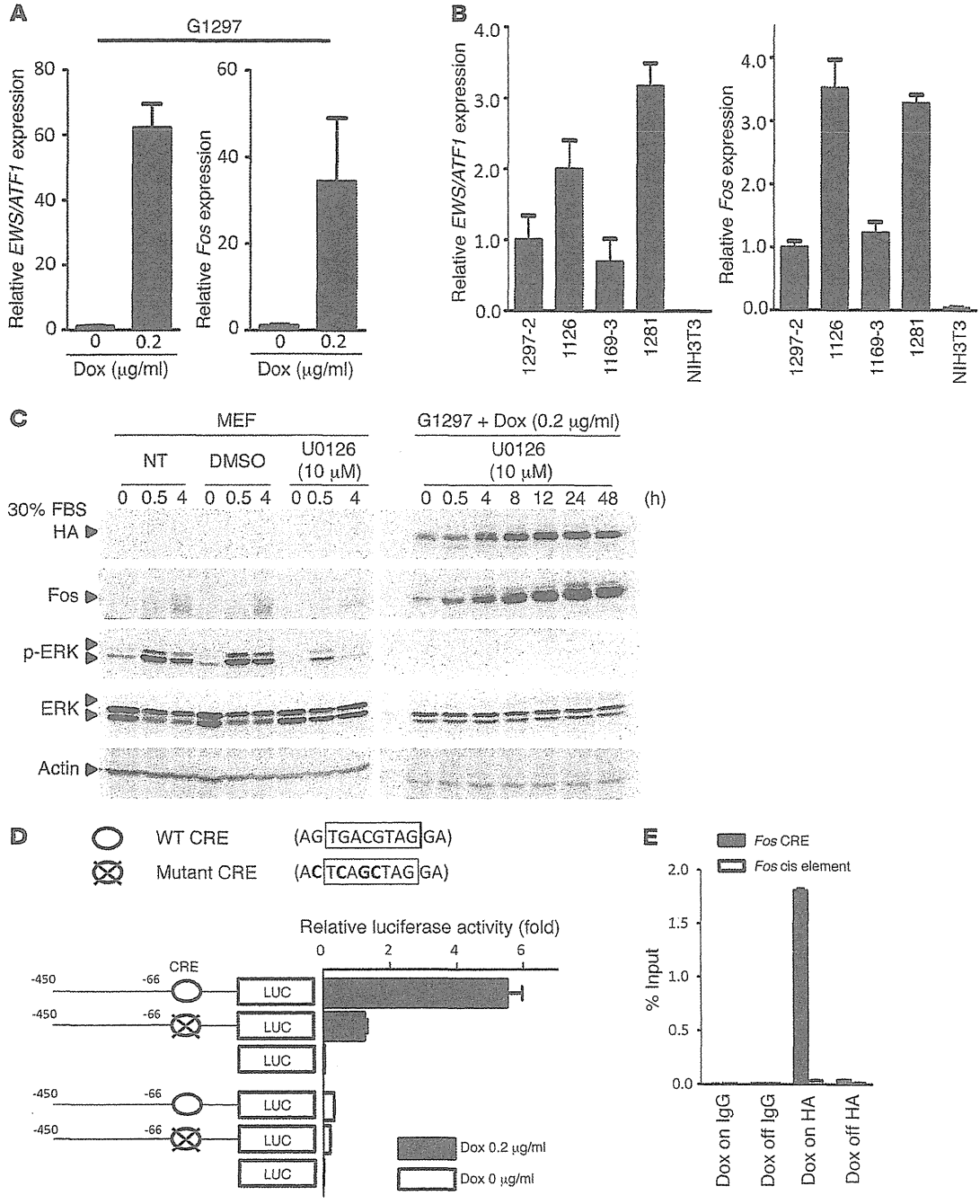

Figure 5

Fos is a direct target of EWS/ATF1. (**A**) Real-time RT-PCR analysis of G1297 cells revealed significant upregulation of both *EWS/ATF1* and *Fos* 3 hours after doxycycline exposure. (**B**) Relative expression of *EWS/ATF1* and *Fos* in 4 *EWS/ATF1*-induced tumors from 4 independent mice. NIH3T3 cells served as a control. Transcript levels were normalized to β-*actin*. Data are mean ± SD ($n = 3$). (**C**) Fos induction by *EWS/ATF1* was independent of the ERK pathway. Serum-starved MEFs and G1297 cells were stimulated with 30% FBS for the indicated times. Cells were also treated with 10 μM of the MEK inhibitor U0126. Whereas ERK1/2 inhibition by U0126 decreased Fos in MEFs, U0126 failed to suppress Fos expression in G1297 cells. NT, not treated. (**D**) Mouse *Fos* promoter–luciferase reporter constructs and pRL-SV40 vector (as an internal control) were cotransfected in G1297 cells treated with or without 0.2 μg/ml doxycycline. Luciferase activity of each construct was normalized to internal control activity. Data are mean ± SD ($n = 3$). (**E**) ChIP-PCR analysis was performed for the *Fos* promoter region containing CRE or the negative control cis element using HA-tag antibody or IgG as nonimmune immunoprecipitation, respectively. EWS/ATF1 was enriched at the CRE element of the *Fos* promoter in G1297 cells after treatment with 0.2 μg/ml doxycycline. Data (mean ± SD) were quantified by qRT-PCR and expressed as percent of input DNA.

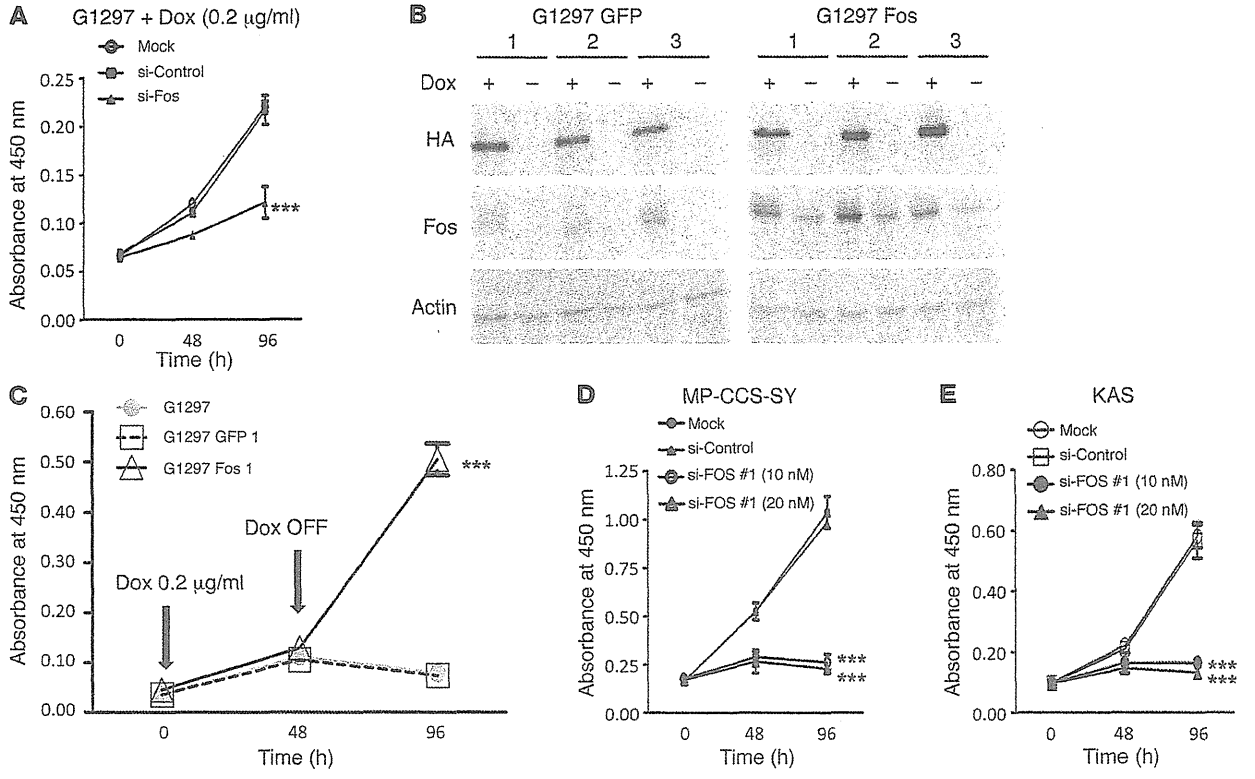

Figure 6

Fos plays a key role in *EWS/ATF1*-induced cell proliferation. (**A**) Effect of *Fos* knockdown on proliferation of *EWS/ATF1*-induced cells. G1297 cells were treated with siRNA targeting *Fos* (si-Fos; 10 nM), a control siRNA (si-Control; 10 nM), or lipofectamine alone (Mock). 48 and 96 hours later, cell viability was determined by WST-8 assay. Results are mean ± SD ($n = 4$). $^{***}P < 0.001$ vs. si-Control and Mock. (**B**) *EWS/ATF1*-induced tumor cell lines overexpressing *Fos* or *EGFP* (G1297 Fos and G1297 GFP, respectively). pCAG-Fos-IZ vector or pCAG-EGFP-IZ vector were stably transfected in G1297 cells. Western blot analysis revealed that G1297 Fos cells stably expressed Fos protein even in the absence of doxycycline. (**C**) Cell proliferation assay for G1297, G1297 GFP, and G1297 Fos cells before and after doxycycline withdrawal. Doxycycline treatment (0.2 μg/ml) was withdrawn for 48 hours. Cell viability was determined by WST-8 assay. $^{***}P < 0.001$ vs. G1297 and G1297 GFP. (**D** and **E**) Effect of *FOS* knockdown on growth of human CCS cell lines. MP-CCS-SY and KAS cells were treated with siRNA#1 targeting *FOS* (si-FOS #1; 10 nM and 20 nM), control siRNA (si-Control; 20 nM), or lipofectamine alone (Mock). 48 and 96 hours later, cell viability was determined by WST-8 assay. Data are mean ± SD ($n = 4$). $^{***}P < 0.001$ vs. si-Control and Mock.

(Supplemental Figure 7D), phosphorylation of ERK1/2 was not observed in the *EWS/ATF1*-induced tumor cell line, even after serum stimulation (Supplemental Figure 7E), which suggests that continuous upregulation of Fos in *EWS/ATF1*-induced tumor cells is independent of the RAS/Raf/ERK signaling pathway. We treated *EWS/ATF1*-induced tumor cells with the MEK inhibitor U0126 to block activation of ERK1/2 in order to further confirm the ERK-independent activation of Fos. Although inhibition of ERK1/2 resulted in a substantial decrease of Fos in MEFs, U0126 failed to suppress Fos expression in *EWS/ATF1*-induced tumor cells (Figure 5C). These data indicate that constitutive overexpression of Fos in *EWS/ATF1*-induced tumor cells was mediated by an ERK-independent mechanism.

Previous studies demonstrated an interaction of ATF1 at a CRE in the *Fos* promoter (34, 35), which suggests that EWS/ATF1 may induce *Fos* expression through interaction with the CRE. Conversely, in the present study, regulatory motif analysis of the upregulated genes by EWS/ATF1 demonstrated enrichment of CRE near the transcription start site (from −1,000 bp to +200 bp; Supplemental Figure 6B). To evaluate the functional importance of this element in EWS/ATF1-mediated activation of *Fos*, we constructed a reporter plasmid containing the mouse *Fos* promoter with wild-type and mutated CRE and examined transcriptional activity by luciferase assay (Figure 5D). We confirmed that induction of EWS/ATF1 resulted in remarkably increased *Fos* promoter activity with wild-type CRE in G1297 cells. Importantly, luciferase activity of the mutated promoter significantly decreased compared with that of the wild-type promoter. We further examined whether EWS/ATF1 directly binds to the CRE of the *Fos* promoter. ChIP-PCR analysis revealed that doxycycline-induced EWS/ATF1 was enriched at the CRE of the *Fos* promoter, but not at the negative control cis element (Figure 5E). Our results indicated that the CRE is crucial for EWS/ATF1-mediated transcriptional activity of *Fos* in *EWS/ATF1*-induced tumor cells.

Expression of FOS in human CCS. To investigate whether overexpression of *FOS* is linked to human CCS, we analyzed *FOS* expression in the human CCS cell lines MP-CCS-SY and KAS and in the control lung fibroblast cell line WI38 by qRT-PCR. *FOS* was found to be highly expressed in both human CCS cell lines compared with WI38 (Supplemental Figure 8A). We also found that surgically resected clinical CCS specimens also expressed higher levels of *FOS* than did WI38 (Supplemental Figure 8B), which indicates that human CCS expresses higher levels of *FOS*.

We examined the effect of *EWS/ATF1* knockdown on *FOS* expression in human CCS cell lines to further investigate the association between *EWS/ATF1* expression and increased *FOS* expression in human CCS. Human CCS cell lines MP-CCS-SY and KAS carry the *EWS/ATF1* type 1 and type 2 fusion genes, respectively (Supplemental Figure 9, A and B). We next designed a specific siRNA targeting the breakpoint of the *EWS/ATF1* type 1 fusion gene, which had no effect on the expression of *ATF1* or of the *EWS/ATF1* type 2 fusion gene in KAS (Supplemental Figure 9, E and F). siRNA treatment targeting *EWS/ATF1* type 1 in MP-CCS-SY led to significant downregulation of *FOS* 48 hours after treatment (Supplemental Figure 9G) as well as of *EWS/ATF1* type 1 itself (Supplemental Figure 9, C and D), which indicates that *FOS* is a direct target of EWS/ATF1 in human CCS. In contrast to *FOS*, we observed a modest reduction of *MITF-M* expression after *EWS/ATF1* knockdown in MP-CCS-SY cells (Supplemental Figure 9H).

FOS could be a promising therapeutic target for human CCS. To examine whether *Fos* overexpression facilitates proliferation of tumor cells expressing *EWS/ATF1*, we knocked down *Fos* in *EWS/ATF1*-induced tumor cells using siRNA. The G1297 cell line was treated with siRNA for *Fos* in the presence of doxycycline. siRNA treatment (10 nM) decreased the expression of *Fos* at the mRNA level by 75% at 24 hours after transfection, although it had no effect on expression of the *EWS/ATF1* transgene compared with the control siRNA (Supplemental Figure 10A). In addition, we confirmed that Fos protein levels were also decreased 48 hours after transfection (Supplemental Figure 10B). A WST-8 assay was performed in *EWS/ATF1*-induced tumor cells transfected with the nonfunctional control siRNA or with functional *Fos* siRNA to examine the effect of *Fos* knockdown on the cellular kinetics. The siRNA targeting *Fos* efficiently inhibited cell proliferation of *EWS/ATF1*-induced tumor cells, even in the presence of doxycycline (Figure 6A). In order to further confirm the importance of *Fos* expression for *EWS/ATF1*-induced tumor cell growth, we established *EWS/ATF1*-induced tumor cell lines in which *Fos* is overexpressed (Figure 6B). We found that *Fos*-overexpressed *EWS/ATF1*-inducible cells retained the ability to proliferate for at least 48 hours after doxycycline withdrawal, whereas control cells in which *GFP* is overexpressed stopped their proliferation soon after withdrawal (Figure 6C). We also examined the effect of *FOS* knockdown on cell growth of human CCS cell lines using siRNA targeting *FOS*. Consistent with the results in *EWS/ATF1*-induced tumor cells, siRNA treatment strongly suppressed the growth of CCS cell lines (Figure 6, D and E, and Supplemental Figure 11, A–F). Taken together, these data suggest that *FOS*, a direct target of EWS/ATF1, mediates the oncogenic growth of *EWS/ATF1*-related sarcomas and could be a potent therapeutic target for human CCS.

Discussion

The current study revealed that forced expression of the *EWS/ATF1* fusion gene induced sarcoma formation in *EWS/ATF1* transgenic mice. The histology of the tumors in *EWS/ATF1* transgenic mice showed a striking similarity to that of human CCS. In addition, immunohistochemistry demonstrated that *EWS/ATF1*-induced tumor cells express neural crest–associated markers, such as S100, Mitf, and Sox10, which are also expressed in human CCS. Given that the *EWS/ATF1* fusion gene is detected in CCS, our *EWS/ATF1* transgenic mouse is the first mouse model for investigating CCS pathogenesis. Our present results demonstrated that continuous expression of *EWS/ATF1* was required for growth and tumor formation of *EWS/ATF1*-induced tumor cells. These results indicate that *EWS/ATF1* plays a pivotal role in both development and maintenance of *EWS/ATF1*-associated sarcomas, implying that CCS exhibits oncogene addiction (36) to *EWS/ATF1*, and provide a rationale for targeting EWS/ATF1 itself to treat CCS.

It is interesting to note that sarcoma formation was observed only in deep soft tissue, although *EWS/ATF1* was induced in a variety of cell types in this experimental system (37, 38). In addition, the cell proliferation rate of MEFs in vitro was reduced by *EWS/ATF1* induction. These results clearly demonstrated that the abnormal proliferation by the forced expression of *EWS/ATF1* requires a specific cell type of origin, accompanied by a specific microenvironment. Consistent with these findings, recent studies of other sarcoma-related genes revealed that introduction of *SYT/SSX*, a synovial sarcoma-related gene, into *Myf5*-positive immature myoblasts specifically resulted in sarcoma formation, whereas its expression in more differentiated cells induced myopathy without tumor induction (39). In addition, introduction of *EWS/FLI1*, a fusion gene detectable in Ewing sarcomas, results in transformation specifically in bone marrow–derived mesenchymal progenitor cells in vitro (40). Taken together, these findings are suggestive of cell type–specific carcinogenesis by expression of sarcoma-related fusion oncogenes.

Our lineage-tracing experiments in vivo suggested that *EWS/ATF1*-associated tumor cells are derived from neural crest–derived cells. This result is consistent with several lines of evidence that CCS often shows melanocytic differentiation and resembles MM. However, our present results do not exclude the possibility that *EWS/ATF1*-induced tumors can arise from non–neural crest–derived cells. In addition, the exact cell type of origin of *EWS/ATF1*-induced tumors remains unclear, since neural crest–lineage progenitors can differentiate into many different cell types, such as neuronal cells, melanocytes, and Schwann cells. Recently, Schwann cell precursors along the peripheral nerve have been shown to be a cellular source of large numbers of melanocytes in the skin during development in mice and chicks (41). Moreover, Schwann cells also retain the potential to differentiate into melanocytes, resulting from a loss of nerve contact (41). Given the finding that *EWS/ATF1*-induced tumor cells expressed markers for melanocytic differentiation, it is possible that the neural crest–derived Schwann cells could be the origin of *EWS/ATF1*-associated sarcomas.

We found that *Fos* was one of the direct targets of EWS/ATF1 in *EWS/ATF1*-induced tumor cells. *Fos* is an immediate early gene that can be activated by a variety of mitogens and growth factors. The present study showed that *Fos* induction by forced expression of *EWS/ATF1* was independent of the ERK signaling pathway. In contrast, we found that *Fos* upregulation was mediated by a CRE of the *Fos* promoter, accompanied by direct interaction of EWS/ATF1 with the CRE on the *Fos* promoter. The direct interaction of EWS/ATF1 at CRE may induce continuous transcriptional activation of *Fos* in *EWS/ATF1*-induced tumor cells. Previous studies have demonstrated a higher expression level of *FOS* to be involved in tumor growth in several cancers (42–44), and overexpression of *Fos* results in osteosarcoma formation in transgenic mice (45, 46). Here we showed that *FOS* was also upregulated in CCS by the *EWS/ATF1* fusion transcript and that the increased *FOS* promoted the growth of *EWS/ATF1*-related sarcomas. Accordingly, blocking the FOS pathway might be a promising therapeutic strategy for treating CCS (Supplemental Figure 12).

Methods

Molecular cloning and gene targeting in ES cells. Human *EWS/ATF1*-FLAG-HA was amplified by RT-PCR from the human CCS cell line KAS using primers ACATGGCGTCCACGGATTACAG and CCTAGGCGTAGTCGGGCACGTCGTAGGGGTATCCTCCAGCGGCCGACTTGTCATCGTCGTCCTTGTAGTCTCCTCCAACACTTTTATTGGAATAAAGAT and cloned into pcr2.1-TOPO. Sequence-verified *EWS/ATF1*-FLAG-HA cDNA was subcloned into a unique *EcoRI* site of pBS31 prime (37, 38). KH2 ES cells (obtained from Open Biosystems) were used to insert a single copy of *EWS/ATF1*-FLAG-HA by Flipase (PLP) recombination into the *Col1A1* locus under the control of a minimal CMV tetracycline-inducible promoter using a previously described method (37), and ES cells were selected for hygromycin resistance.

Mouse generation. For blastocyst injections, fertilized zygotes were isolated from the oviducts of day-0.5 pregnant B6D2F1 females and allowed to develop to the blastocyst stage in culture. 7–12 ES cells were injected per blastocyst. The injected blastocysts were transferred into day-2.5 pseudopregnant recipient females.

Doxycycline treatment. 6-week-old mice were administered 50 μg/ml doxycycline (Sigma-Aldrich) in their drinking water supplemented with 2 mg/ml sucrose. For cultured cells, doxycycline was used at a concentration of 0.05–0.2 μg/ml.

RNA preparation and RT-PCR. Total RNA was isolated using a RNeasy mini kit (Qiagen). Total RNA was reverse transcribed using a High-Capacity cDNA Reverse Transcription Kit with RNase inhibitor (Applied Biosystems). qRT-PCR analysis using the fluorescent SYBR green method (Bio-Rad) was performed in accordance with the manufacturer's instructions. The data generated from each reaction were subjected to gene expression analysis using an iCycler iQ Real-Time PCR Detection System (Bio-Rad). See Supplemental Table 1 for specific primer pairs used for amplification. Microarray analysis was performed with SurePrint G3 Mouse GE 8X60K microarray (Agilent Technologies) and Mouse Gene 1.0 ST Array (Affymetrix) according to the manufacturer's instructions. All analyses were performed by Genespring GX (version 12; Agilent Technologies).

Western blot analysis. Western blot analyses were carried out as described previously (47, 48). The following antibodies were used: anti-HA (rabbit IgG, 1:1,000 dilution; Cell Signaling), anti-Fos (rabbit IgG, 1:1,000 dilution; Cell Signaling), anti-ERK1/2 (rabbit IgG, 1:1,000 dilution; Cell Signaling), anti-phospho-ERK1/2 (rabbit IgG, 1:1,000 dilution; Cell Signaling), anti-ATF1 (rabbit IgG, 1:5,000 dilution; EPITOMICS), and anti-β-actin (mouse IgG, 1:5,000 dilution; Calbiochem).

Cell proliferation assay. Cell growth was determined by WST-8 assay using a Cell Counting Kit-8 (Dojindo Laboratories). Absorbance at 450 nm is indicative of the die amount of formazan, which is directly proportional to the number of living cells.

Histological analysis. Normal and tumor tissue samples were fixed in 10% buffered formalin for 24 hours and embedded in paraffin. 4-μm sections were stained with H&E, and serial sections were used for immunohistochemical analyses. Immunostaining was performed using an avidin-biotin immunoperoxidase assay. The primary antibodies used were anti-HA-Tag (1:600 dilution; Cell Signaling), anti-Ki67 (1:250 dilution; Dako), anti-S100 (1:800 dilution; Dako), anti-SOX10 (1:200 dilution; R&D Systems), anti-MITF (1:500 dilution; Exalpha), and anti-GFP (1:1,000 dilution; Abcam).

X-gal staining. Briefly, tumor tissue samples were embedded in OCT compound and frozen. 8-μm cryostat sections were immediately fixed in 0.2% glutalaldehyde for 10 minutes. The sections were stained overnight in an X-gal staining solution, then counterstained with fast red for 3 minutes.

Tumorigenicity studies. 4-week-old male BALB/c athymic mice were obtained from Japan SLC. A total of 5.0×10^6 G1297 cells in 0.1 ml serum-free DMEM was inoculated subcutaneously through a 26-gauge needle into the posterior flank of each mouse. 3 weeks after inoculation, the tumor diameters were measured with digital calipers, and tumor volume was calculated as $(w^2 \times l)/2$ and expressed in mm^3.

siRNA transfection. We performed transient knockdown assays with a siRNA targeting *Fos* (Santa Cruz), *FOS* (Santa Cruz and Dharmacon) or the breakpoint of *EWS/ATF1* type 1 (sense, GCGGUGGAAUGGGAAAAAUTT; antisense, AUUUUUCCCAUUCCACCGCTT; KOKEN) using Lipofectamine RNAiMAX (Invitrogen). We used nontargeting siRNA (Cosmo Bio Co.) as a control.

Cell lines. MP-CCS-SY and KAS are CCS cell lines carrying *EWS/ATF1* type 1 and type 2, respectively. MP-CCS-SY was established as described previously (49), and KAS was provided by T. Nakamura (Cancer Institute, Japanese Foundation for Cancer Research, Tokyo, Japan; ref. 24). HOS (osteosarcoma), U2OS (osteosarcoma), NIH3T3 (embryonic fibroblast), and WI38 (lung fibroblast) cells were purchased from the American Type Culture Collection. B16-F1 (mouse melanoma) and A375 (human MM) were purchased from the European Collection of Cell Cultures.

Mice. Wnt1-Cre mice were provided by S. Iseki (Tokyo Medical and Dental University, Tokyo, Japan; ref. 50), *P0-Cre* mice were provided by K. Yamamura (Kumamoto University, Kumamoto, Japan; ref. 51), and floxed *LacZ* mice were provided by M. Okabe (Osaka University, Suita, Japan; ref. 52). Floxed *EYFP* mice (53) were obtained from Jackson Laboratory.

Construction of the reporter plasmid. To obtain the *Fos* reporter plasmid (pGL3A-1486), the genomic DNA fragment containing −450 to +0 of the 5′-flanking sequence was amplified by PCR with the primer set 5′-TCTATCGATAGGTACGAATGTTCGCTCGCCTTCTC-3′ and 5′-ACGCGTAAGAGCTCGGGAGTAGTAGGCGCCTCAGC-3′ and subcloned into the *KpnI* site of the pGL3 vector (Promega). The *Fos* reporter plasmid with mutant CRE element was generated by PCR-targeted mutagenesis with the primer set 5′-CCAGTTCCGCCCACTCAGCTAGGAAGTCCATCC-3′ and 5′-GGATGGACTTCCTAGCTGAGTGGGCGGAACTGG-3′.

Luciferase assay. Reporter genes were transfected into the G1297 *EWS/ATF1*-induced tumor cell line together with phRL-SV40 (Promega) using lipofectamine LTX (Invitrogen), and luciferase activity was measured with a luminometer (VERITAS; Promega). Firefly luciferase activities, derived from each reporter construct, were normalized to Renilla luciferase activities from phRL-SV40.

Stable transfection. To obtain *Fos* expression plasmid (pCAG-Fos-IZ vector), *Fos* cDNA was amplified by RT-PCR from the G1297 cell line with the primer set 5′-ACATGATGTTCTCGGGTTTCAA-3′ and 5′-ACTCACAGGGCCAGCAGCGTGG-3′ and subcloned into the *ECoR* site of the pCAG-*EGFP*-IZ vector (provided by H. Niwa, RIKEN, Kobe, Japan). pCAG-*EGFP*-IZ vector or pCAG-*Fos*-IZ vector was transfected into the G1297 cell line using Lipofectamine LTX Reagent (Invitrogen) and selected for Zeocine resistance (600 μg/ml).

Patients and tumor tissue collection. Anonymized tumor specimens were obtained by surgical resection or biopsy at Gifu University Hospital or Kyoto University Hospital in accordance with an approved protocol from the Institutional Review Board. Total RNA was isolated using a RNeasy mini kit (Qiagen).

ChIP analysis. A total of 5.0×10^6 *EWS/ATF1*-inducible tumor cells was fixed in 1% formaldehyde for 10 minutes, followed by treatment with 1 ml glycine buffer for 5 minutes. Cells were pelleted, washed, and then resuspended in lysis buffer for 30 minutes. After centrifugation, the pellet was resuspended in NP40 buffer with protease inhibitors (Sigma-Aldrich). Sonication was performed using a XL-2000 (MISONIX), after which the supernatant was used as the input sample for immunoprecipitation experiments. Antibodies used were rabbit HA (Cell Signaling) and rabbit normal IgG (Abcam). Protein G–coated magnetic beads were used to purify specific antibody/DNA complexes. After washes, immunoprecipitated DNA was decrosslinked by elu-